Antarctic Science 18 (3), 357–376 (2006) © Antarctic Science Ltd Printed in the UK DOI: 10.1017/S0954102006000411

New petrographic and geochemical insights on diagenesis and palaeoenvironmental stress in Late Cretaceous inoceramid shells from the James Ross Basin, Antarctica

ÁLVARO JIMÉNEZ-BERROCOSO[1], EDUARDO B. OLIVERO[2] and JAVIER ELORZA[1,*]

[1]*Departamento de Mineralogía y Petrología, Universidad del País Vasco, Apartado 644, E-48080 Bilbao, Spain*
[2]*Centro Austral de Investigaciones Científicas (CADIC-CONICET), 9410 Ushuaia, Tierra del Fuego, Argentina*
**Author for correspondence: nppelzaj@lg.ehu.es*

Abstract: New petrographic and geochemical insights from inoceramid bivalve shells of lower Campanian (Marambio Group, James Ross Basin, Antarctica) show that they suffered significant palaeoenvironmental stress just before their disappearance in the southern high latitudes. Inoceramid data have mainly been derived from shell fragments of the large form *Antarcticeramus rabotensis* Crame & Luther, collected at stratigraphical levels marking the early disappearance of inoceramids in the James Ross Basin (10 m.y. before the Cretaceous/Tertiary boundary in Antarctica). Cathodoluminescence studies and minor and trace element intra-shell variations in *A. rabotensis* shells, along with their whole shell geochemistry (major, minor, and trace elements, including REE), have revealed evidence of only weak diagenesis but significant palaeoenvironmental stress. The most relevant evidence of such adverse palaeoenvironmental conditions in *A. rabotensis* shells is reflected by marked growth interruptions in the normal shell layering, including the occurrence of a previously undetected inner aragonitic nacreous layer formed of alternating aragonitic and calcitic sublayers. The weak diagenesis produced characteristic geochemical intra-shell variations, which have subsequently been detected in the inoceramid shell microstructure, especially in the inner aragonitic nacreous layer.

Received 7 April 2005, accepted 15 March 2006

Key words: Campanian, cathodoluminescence, geochemistry, inoceramid extinction, low Mg calcite microstructure, shell growth

Introduction

New insights into the early disappearance of inoceramids in the Southern Hemisphere, apparently related to global, long-lasting palaeoenvironmental changes throughout the Late Cretaceous are presented in this paper. For over twenty years, these palaeoenvironmental changes in the southern high latitudes have triggered debates in palaeontological and geochemical research. Stable isotopic data gathered from molluscs (ammonites, belemnites and bivalves) (Pirrie & Marshall 1990a, 1990b, Marshall *et al.* 1993, Ditchfield *et al*. 1994) and microfossils (planktonic and benthic foraminifers) (Barrera *et al*. 1987, Barrera & Huber 1990, D'Hondt & Lindinger 1994, Huber *et al*. 1995, Li & Keller 1999, Barrera & Savin 1999), along with studies of growth rings in fossil wood (Francis 1986, 1989) and climate related geochemical variations in sediments (Dingle & Lavelle 1998), are all consistent with a climatic cooling trend in high latitudes, both in the oceanic waters and terrestrial environments of the Southern Hemisphere during the Late Cretaceous (Huber 1998, Huber *et al*. 2002). The main causes for these global palaeoenvironmental changes are not well understood, although the evidence suggests that they may have been related to high organic production in shallow waters at low-latitudes, with a consequent reduction in atmospheric CO_2 (Spicer & Corfield 1992).

The inferred long-term cooling and associated changes in stratification of the oceanic water column at high latitudes during the Late Cretaceous are thought to have exerted a profound influence on Antarctic marine organisms. Changes in the diversity and composition of micro- and macrofauna, along with their early disappearance and migration events, appear to reflect alterations in the marine palaeoenvironment around Antarctica (Huber & Watkins 1992, Huber *et al*. 1995, Olivero & Medina 2000). The Cretaceous thermal maximum (Turonian–Coniacian) is detectable in the Hidden Lake Formation. Temperatures then decline from some point in the Campanian to the late Maastrichtian. They fluctuate over the Cretaceous/Tertiary (K/T) boundary, but then rise through the Palaeocene to the Palaeocene–Eocene boundary (PETM) (J.A. Crame, personal communication 2005). Especially relevant for the present contribution is the early disappearance of inoceramids in Antarctica (Crame *et al*. 1996). This group was well represented from the Aptian up to the Santonian–earliest Campanian in the James Ross Basin (Antarctica) (Crame 1983, Scasso *et al*. 1991, Medina & Buatois 1992). However, the group declined during the early Campanian, reappeared in the late early Campanian (Scasso *et al*. 1991, Olivero 1992), with the abundant occurrence of the large species *Antarcticeramus rabotensis*

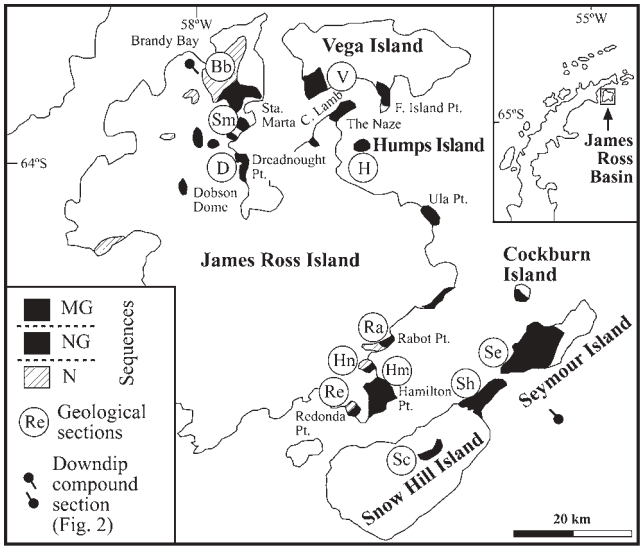

Fig. 1. General map of the James Ross Basin area, Antarctica, with the distribution of the *Natalites* Sequence (N Sequence, Santonian–early Campanian), *Neograhamites-Gunnarites* Sequence (NG Sequence, late Campanian–early Maastrichtian), and *Maorites-Grossouvrites* Sequence (MG Sequence, Maastrichtian). Circled letters represent sections studied in this study (Bb = Brandy Bay, Sm = Santa Marta, V = Vega, H = Humps, D = Dreadnought, Ra = Rabot, Re = Redonda, Hn = north Hamilton, Hm = Hamilton, Sc = Sanctuary Cliffs, Sh = Snow Hill and Se = Seymour Island). Adapted from Olivero *et al*. (1999), Olivero & Medina (2000) and Elorza *et al*. (2001).

Crame & Luther (Crame *et al*. 1996, Crame & Luther 1997), and finally completely disappeared from the James Ross Basin in the basal late Campanian (Figs 1 & 2). A similar timing for the early disappearance of the inoceramids has also been found in deep marine deposits in Tierra del Fuego (Olivero *et al*. 2003, 2004).

In lower latitudes of the Northern Hemisphere, inoceramids disappeared at the early/late Maastrichtian boundary (MacLeod *et al*. 1996, 2000, Gómez-Alday *et al*. 2004). In the deep water pelagic limestone of Umbria–Marche Apenines (Italy), inoceramids disappeared synchronously about 3.5 m.y. before the K/T boundary (69.1 m.y., magnetic chron C31R), which is about 0.9 m.y. before the inoceramid extinction in the Basque–Cantabrian Basin (Spain) (68.2 m.y., mid part of magnetic chron C31N, using the time scale of Cande & Kent (1995)). Therefore, on a global scale, inoceramid extinction was diachronous, encompassing at least a 4 m.y. interval between the last appearance datum at several DSDP sites and the last appearance datum at the Sopelana sections (Basque–Cantabrian Basin) (Chauris *et al*. 1998, and references therein). This diachronous extinction of inoceramids cannot be explained by a global catastrophic event, such as a large cosmic impact, exceptional volcanic eruptions or eustacy. On the contrary, the primary causes have been suggested to be long-lasting palaeoecological changes, probably driven by climatic changes during the Late Cretaceous (MacLeod *et al*. 1996).

Elorza *et al*. (2001) demonstrated varying degrees of diagenetic modification in the Campanian inoceramid shells from the James Ross Basin, recorded both by cathodoluminescence (CL) observation and light isotopic values ($\delta^{18}O$). However, the prominent growth breaks recorded by these authors in the *A. rabotensis* shell microstructure under petrographic observation seem to

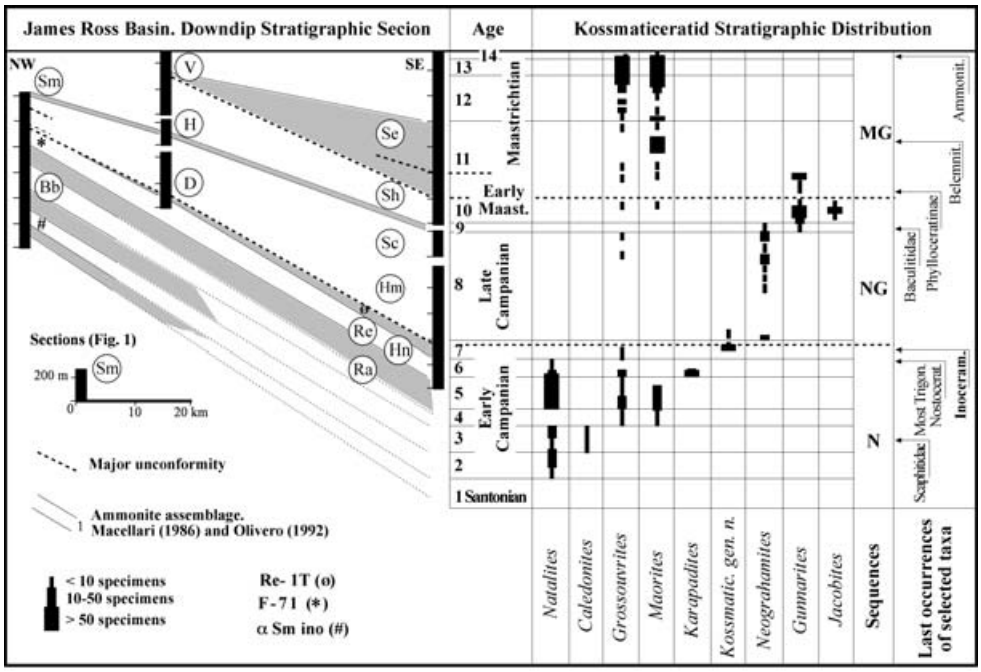

Fig. 2. Compound section of the Late Cretaceous James Ross Basin showing the stratigraphical distribution of the principal ammonites (Kossmaticeratidae family) and the main stratigraphic levels recording the last occurrences of selected mollusc taxa. Key for sedimentary sections is shown in Fig. 1. Figure adapted from Olivero & Medina (2000) and Elorza *et al*. (2001).

https://doi.org/10.1017/S0954102006000411 Published online by Cambridge University Press

reflect the response of the organisms to marked changes in palaeoenvironmental conditions, which could eventually have led to the early disappearance of the group in Antarctica. Furthermore, different stable oxygen isotope values from early Campanian and Maastrichtian belemnites confirm a temperature drop during this interval, which supports inferences of increasing palaeoenvironmental stress as a likely explanation for the early inoceramid disappearance, about 10 m.y. before the K/T boundary in Antarctica (Elorza *et al*. 2001).

In this study, new geochemical microprobe and whole-sample analyses, together with petrographic studies are presented, on the early to basal late Campanian inoceramids and host rocks from the James Ross Basin, with the aim of inferring their geochemical response to both diagenesis and palaeoenvironmental changes. Our data have confirmed that earliest Campanian inoceramids show a regular microstructure, whereas latest early Campanian-basal late Campanian specimens exhibit marked microstructural anomalies and previously undetected geochemical changes across the shell layering, the latter a likely consequence of palaeoenvironmental stress just before the early disappearance of the group in Antarctica.

Geological setting

A major Cretaceous–Palaeogene marine sedimentary succession, with a thickness in excess of 6 km, is preserved in the James Ross Basin (north-east Antarctic Peninsula) (Fig. 1). The evolution of deep marine environments during the Early Cretaceous (Ineson 1989) to shelf settings during the Late Cretaceous–Palaeogene is recorded in this back-arc basin (Scasso *et al*. 1991, Pirrie 1991, Olivero *et al*. 1992, Crame *et al*. 2004). Within the Late Cretaceous–Palaeogene, the Santonian–Danian succession is relatively complete, highly fossiliferous, includes the K/T boundary, and represents a unique geological window for the study of biotic and palaeoenvironmental changes in the southern high latitudes (Macellari 1986, Olivero 1992, Zinsmeister & Feldmann 1996, Olivero & Medina 2000).

The Santonian–Maastrichtian–Danian succession is contained within the Marambio Group (Fig. 2), which is about 3 km thick, and mainly composed of sandy and silty mudstones, with subordinate sandstones, coquinas and conglomerates (Macellari 1988, Scasso *et al*. 1991, Olivero *et al*. 1992, Pirrie *et al*. 1997). Due to the dominance of homogeneous fine-grained sediments, there is no general agreement on the stratigraphic division of the Marambio Group. Therefore, herein we follow the allostratigraphic division of Olivero *et al*. (1999) and Olivero & Medina (2000). Accordingly, three main stratigraphic sequences are included in the Marambio Group:

a) the N Sequence (Santonian–early Campanian),

b) the NG Sequence (late Campanian–early Maastrichtian), and

c) the MG Sequence (mid-Maastrichtian–Danian).

The sequence names are derived from their most abundant kossmaticeratid genera:

a) *Natalites* (N Sequence),

b) *Neograhamites-Gunnarites* (NG Sequence), and

c) *Maorites-Grossouvrites* (MG Sequence).

The base and top of the NG Sequence are defined by two important regional unconformities, which are accompanied by notable changes in the diversity and composition of marine invertebrate biota (Olivero & Medina 2000) (Fig. 2).

Materials and methods

The studied material, comprising samples of inoceramid shell and host rock, was collected from different stratigraphic horizons of the N Sequence (Santonian–early Campanian), specifically at the Brandy Bay, Santa Marta and Redonda Point sections (James Ross Island) (Figs 1 & 2). The material from lower stratigraphic horizons of the N Sequence, at the Brandy Bay section, includes several specimens of *Dimitobelus* sp. (belemnites) and *Inoceramus* sp. (sample SM), recorded within the *Inoceramus* Biofacies (Scasso *et al.* 1991), *Natalites rossenssis* Assemblage (ammonite assemblage 2), and Alpha Member (earliest Campanian part of the Santa Marta section). The material from higher stratigraphic horizons of the N Sequence at the Brandy Bay section are specimens of *Dimitobelus* sp. and the inoceramid *A. rabotensis* Crame & Luther (sample I-1), found close to the boundary between ammonite assemblages 6 and 7 of latest early Campanian age (Fig. 2) (Olivero 1992, Olivero & Medina 2000). The rest of the material from the N Sequence at the Brandy Bay section includes several specimens of *Dimitobelus* sp. recorded at intermediate stratigraphic levels of early Campanian age and specimens of *A. rabotensis* (sample F-71) of latest early Campanian age. The material from the N Sequence at the Redonda Point section includes specimens of *A. rabotensis* (samples I-2, I-3, I-4, I2-ino, Re (a), Re-b, Re-1T and Re 4/5), also of latest early Campanian age.

A total of 30 thin sections of inoceramid shells were studied by standard transmitted light microscopy and CL. All CL work employed a Technosyn Cold Cathode Luminescence system, model 8200 MK II, mounted on an Olympus triocular research microscope with a maximum magnification capability of 400x using universal stage objectives. Standard operating conditions included an accelerating potential of 12 kV and a 0.5–0.6 mA beam current with a focused beam diameter of approximately 5 mm. Fragments of inoceramid shells were also selected and examined under the scanning electron microscope (SEM). Inoceramid prismatic microstructure with

https://doi.org/10.1017/S0954102006000411 Published online by Cambridge University Press

Table I. Minor and trace element mean values (mmol/mol) for *A. rabotensis* Re-1T and F-71 shells, along the microprobe transects (Line 1 and Line 2). Geochemical data are presented as (intra-) prismatic non-luminescent and luminescent points, aragonitic and calcitic sublayers, and inter-prismatic luminescent points.

		Mg/Ca	Sr/Ca	Na/Ca	Ba/Ca	Fe/Ca	Mn/Ca
A. rabotensis Re-1T (analysis interval)							
Line 1	Zone 1, non-luminescent (1 to 48)	5.61 ± 1.3	1.63 ± 0.5	7.97 ± 1.9	0.18 ± 0.2	0.25 ± 0.3	0.15 ± 0.2
	Zone 2, luminescent (49 to 169)	9.80 ± 4.3	1.39 ± 0.7	5.12 ± 4.1	0.19 ± 0.3	8.07 ± 6.3	8.95 ± 6.2
Line 2	Zone 1, non-luminescent (1 to 99)	7.10 ± 2.2	1.64 ± 0.4	8.08 ± 2.4	0.18 ± 0.2	0.64 ± 0.4	0.37 ± 0.2
	Zone 2, luminescent (100 to 193)	11.28 ± 4.8	1.37 ± 0.6	4.60 ± 2.5	0.18 ± 0.3	7.58 ± 5.8	8.29 ± 6.4
	Inter-prismatic zones, luminescent	6.68 ± 2.4	0.79 ± 0.5	5.42 ± 3.6	0.05 ± 0.1	5.00 ± 2.8	5.23 ± 3.1
A. rabotensis F-71 (analysis interval)							
Line 1	Zone 1, luminescent (1 to 8)	26.45 ± 7.7	1.95 ± 1.0	4.37 ± 1.3	0.12 ± 0.2	4.69 ± 1.5	3.93 ± 2.0
	Zone 2, non-luminescent (9 to 145)	5.33 ± 2.3	1.90 ± 0.6	7.54 ± 2.7	0.17 ± 0.2	0.28 ± 0.5	0.23 ± 0.5
	Zone 3, aragonitic sublayer (146 to 149)	0.28 ± 0.4	5.20 ± 0.4	10.33 ± 4.3	0.00	0.15 ± 0.2	0.06 ± 0.1
	Zone 4, calcitic sublayer (150 to 151)	1.70 ± 1.6	2.26 ± 0.4	11.71 ± 0.7	0.15 ± 0.2	3.25 ± 3.7	0.00
	Zone 5, aragonitic sublayer (152 to 154)	0.13 ± 0.2	4.17 ± 0.1	9.94 ± 1.4	0.01 ± 0	0.35 ± 0.3	0.44 ± 0.2
	Zone 6, calcitic sublayer (155 to 157)	2.04 ± 2.0	8.88 ± 7.0	10.78 ± 4.3	0.43 ± 0.5	3.80 ± 4.9	0.00
	Zone 7, aragonitic sublayer (152 to 160)	0.70 ± 1.1	6.46 ± 4.9	16.27 ± 10.9	0.25 ± 0.3	0.62 ± 1.0	0.20 ± 0.2
	Zone 8, calcitic sublayer (161 to 164)	10.73 ± 6.1	2.77 ± 2.4	5.56 ± 2.6	0.47 ± 0.6	3.29 ± 3.6	4.44 ± 4.6
	Zone 9, aragonitic sublayer (165 to 167)	0.53 ± 0.4	6.91 ± 0.7	10.14 ± 0.3	0.11 ± 0.2	1.54 ± 1.2	0.03 ± 0.1
	Zone 10, calcitic sublayer (168 to 169)	14.97 ± 5.5	5.15 ± 1.6	10.31 ± 1.0	0.00	8.00 ± 0	0.34 ± 0.2
	Inter-prismatic zones, luminescent	13.50 ± 6.3	1.79 ± 0.8	9.12 ± 10.9	0.18 ± 0.3	1.93 ± 1.2	1.60 ± 0.7
Line 2	Zone 1, non-luminescent, (1 to120)	5.37 ± 1.8	1.80 ± 0.6	6.86 ± 1.7	0.19 ± 0.3	0.20 ± 0.4	0.19 ± 0.2
	Zone 2, aragonitic sublayer, (121 to 122)	2.95 ± 4.2	6.83 ± 0.1	7.47 ± 0.1	0.35 ± 0.2	1.13 ± 0.4	1.85 ± 2.0
	Zone 3, calcitic sublayer (123 to 127)	5.25 ± 3.2	1.93 ± 1.4	6.85 ± 8.3	0.23 ± 0.2	2.04 ± 4.1	0.16 ± 0.2
	Zone 4, aragonitic sublayer (128 to 136)	0.83 ± 1.7	5.85 ± 2.3	9.51 ± 1.5	0.23 ± 0.3	1.27 ± 2.7	0.16 ± 0.2
	Inter-prismatic zones, luminescent	22.68 ± 7.5	1.30 ± 0.2	5.17 ± 3.0	0.16 ± 0.2	4.85 ± 4.5	5.73 ± 5.0
		Mg	Sr	Na	Ba	Fe	Mn
	Detection limits (ppm)	166	569	302	~1	411	~1
	Counting times (sec)	15	30	15	30	15	15

anomalous glauconite-rich layers was detected under standard transmitted light and qualitatively determined (Al, Si, Fe, Mg, K) by energy dispersive spectrometry (SEM/EDX) using a Jeol JSM-T6400 (University of the Basque Country).

Two inoceramid shell samples (*A. rabotensis* Re-1T and F-71) were analysed by electron probe microanalyser (EPMA) to determine Ca^{2+}, Mg^{2+}, Sr^{2+}, Na^{+}, Ba^{2+}, Fe^{2+} and Mn^{2+} contents (Cameca SX100 electron microprobe at the Département des Sciences de la Terre of the Université Blaise Pascal, Clermont-Ferrand, France). Analytical conditions were a beam current of 30 nA for all of the elements, except Ca^{2+} (10 nA), an accelerating voltage of 15 kV and a spot diameter of 5 µm, which can be easily observable in reflected light and under CL. Details of the analytical conditions (detection limits and counting times) are given in Jiménez-Berrocoso *et al*. (2004) and Table I. Analyses of the shell samples totalled 667 spots, shared in four transects corresponding to shells *A. rabotensis* Re-1T (Line 1 and Line 2) and F-71 (Line 1 and Line 2), typically along the prisms of the inoceramid shells. Analysis intervals, between 10 and 20 microns apart, varied according to the thickness of the shells and the growth lines, due to the occasional difficulty in recognizing the finest growth lines. All the analyses were then related to their location within the shell and to the CL emission (outer and inner shell layers, inter-prismatic zones) using thin section photographs in both reflected light and CL.

Three inoceramid shell samples (*A. rabotensis* Re-1T and F-71 and *Inoceramus* sp. SM) and associated host rock were further examined for their contents of major, minor and trace elements (32 elements) and REE (14 elements). Whole samples (inoceramid shell and host rock) were powdered in a tungsten-carbide mill. Major elements (wt %) were determined by inductively coupled plasma (ICP) emission spectrometry. Samples for trace element and REE analyses were fused with ultrapure lithium metaborate flux, dissolved while molten in HNO_3, and analysed on a VG PlasmaQuad PQ22, inductively coupled plasma source mass spectrometer (ICP-MS) at the Centre de Recherches Pétrographiques et Géochimiques (Nancy, France), following techniques described by Govindaraju & Mevelle (1987). The detection limits are incorporated in Tables II & III.

Morphologic and petrographic features of inoceramid shells

The large specimens of *A. rabotensis*, from the Brandy Bay and Redonda Point sections (top of N Sequence), were previously recorded as "big *Inoceramus*" in Olivero *et al*. (1986), Lirio *et al*. (1989), Crame *et al*. (1991), Marenssi

https://doi.org/10.1017/S0954102006000411 Published online by Cambridge University Press

Table II. Whole-sample geochemistry (major, minor and trace elements) for inoceramid shells (Ino) (*Inoceramus* sp. and *A. rabotensis*) and host rock (Hr). Analytical detection limits (d.l.) are presented in brackets.

Elements (detection limits)	*A. rabotensis* F-71(Ino)	Host rock F-71(Hr)	*A. rabotensis*/ host rock F-71(Ino)/F-71(Hr)	*A. rabotensis* Re-1T (Ino)	Host rock Re-1T (Hr)	*A. rabotensis*/ host rock Re-1T(Ino)/Re-1T(Hr)	*Inoceramus* sp. SM(Ino)	Host rock SM(Hr)	*Inoceramus* sp./ host rock SM(Ino)/SM(Hr)
SiO_2 (0.2%)	< d.l.	28.97	-	< d.l.	35.30	-	0.49	32.35	0.02
Al_2O_3 (0.1%)	< d.l.	6.22	-	< d.l.	5.60	-	0.46	7.40	0.06
Fe_2O_3 (0.1%)	< d.l.	3.72	-	< d.l.	1.98	-	< d.l.	3.07	-
MnO (0.03%)	0.06	0.50	0.12	0.07	0.53	0.13	0.11	0.28	0.39
CaO (0.15%)	51.68	30.20	1.71	54.51	30.27	1.80	50.61	27.68	1.83
MgO (0.15%)	0.31	1.11	0.28	0.31	0.35	0.89	0.91	1.17	0.78
Na_2O (0.05%)	0.17	0.77	0.22	0.32	1.14	0.28	0.46	1.38	0.33
K_2O (0.05%)	< d.l.	1.22	-	< d.l.	1.10	-	< d.l.	1.20	-
TiO_2 (0.05%)	< d.l.	0.25	-	< d.l.	0.28	-	< d.l.	0.39	-
P_2O_5 (0.05%)	< d.l.	0.39	-	< d.l.	6.32	-	0.31	15.05	0.02
Rb (0.60 ppm)	< d.l.	48.76	-	0.73	39.28	0.02	1.05	45.58	0.02
Cs (0.20 ppm)	< d.l.	1.92	-	< d.l.	1.35	-	< d.l.	1.63	-
Sr (2.00 ppm)	1236	300	4.12	1069	753.90	1.42	1362	418.60	3.25
Ba (2.00 ppm)	4.06	253.8	0.02	59.59	371.70	0.16	11.28	229.80	0.05
Y (0.1 ppm)	3.40	14.58	0.23	6.32	43.70	0.14	5.13	265	0.02
Zr (1.00 ppm)	1.19	97.26	0.01	1.22	92.12	0.01	4.37	134.80	0.03
Hf (0.04 ppm)	< d.l.	2.56	-	< d.l.	2.34	-	0.09	2.86	0.03
V (1.50 ppm)	< d.l.	52.46	-	< d.l.	41.33	-	2.03	63.95	0.03
Nb (0.10 ppm)	< d.l.	4.21	-	< d.l.	4.14	-	0.12	4.70	0.02
Ta (0.02 ppm)	< d.l.	0.38	-	< d.l.	0.37	-	< d.l.	0.44	-
Cr (5.00 ppm)	< d.l.	18.77	-	< d.l.	25.95	-	< d.l.	15.82	-
Co (0.20 ppm)	0.74	5.08	0.15	0.83	5.09	0.16	0.96	4.42	0.22
Ni (6.00 ppm)	8.03	12.53	0.64	7.50	11.16	0.67	8.60	10.10	0.85
Cu (4.00 ppm)	< d.l.	7.30	-	< d.l.	6.86	-	< d.l.	6.17	-
Zn (8.00 ppm)	< d.l.	64.11	-	< d.l.	34.34	-	9.47	65.98	0.14
Ga (0.15 ppm)	< d.l.	8.38	-	0.19	6.78	0.03	0.38	13.12	0.03
Sn (0.50 ppm)	0.54	1.20	0.45	< d.l.	0.97	-	< d.l.	1.43	-
Pb (1.50 ppm)	< d.l.	16.14	-	1.71	10.74	0.16	3.76	10.48	0.36
As (0.70 ppm)	< d.l.	4.08	-	< d.l.	7.96	-	< d.l.	3.65	-
Bi (0.05 ppm)	< d.l.	0.12	-	< d.l.	0.08	-	< d.l.	0.12	-
Th (0.05 ppm)	0.06	4.18	0.01	0.50	3.98	0.12	0.11	4.78	0.02
U (0.05 ppm)	0.41	1.17	0.35	0.20	2.29	0.09	0.37	9.07	0.04

Table III. REE results for inoceramid shells (Ino) (*Inoceramus* sp. and *A. rabotensis*) and host rock (Hr). Analytical detection limits (d.l.) are presented in brackets.

Elements (detection limits)	*A. rabotensis* F-71(Ino)	Host rock F-71(Hr)	*A. rabotensis*/ *host rock* F-71Ino/Hr	*A. rabotensis* Re-1T(Ino)	Host rock Re-1T(Hr)	*A. rabotensis*/ *host rock* Re-1T(Ino/Hr)	*Inoceramus* sp. SM(Ino)	Host rock SM(Hr)	*Inoceramus* sp./ *host rock* SM(Ino/Hr)
La (0.10 ppm)	1.18	12.7	0.09	4.03	51.9	0.08	10.70	325	0.03
Ce (0.10 ppm)	2.92	26.8	0.11	9.56	60.50	0.16	18.00	597	0.03
Pr (0.03 ppm)	0.281	3.07	0.09	0.976	5.45	0.18	1.78	64.90	0.03
Nd (0.10 ppm)	1.24	11.9	0.10	3.96	19.50	0.20	6.88	256	0.03
Sm (0.10 ppm)	0.325	2.49	0.13	0.953	3.67	0.26	0.986	41.50	0.02
Eu (0.01 ppm)	0.081	0.543	0.15	0.237	6.60	0.03	0.149	6.35	0.02
Gd (0.10 ppm)	0.387	2.16	0.18	0.971	4.30	0.22	0.802	35.90	0.02
Tb (0.03 ppm)	0.069	0.342	0.20	0.179	0.61	0.29	0.096	4.80	0.02
Dy (0.10 ppm)	0.462	2.06	0.22	1.07	3.60	0.30	0.546	28.40	0.02
Ho (0.03 ppm)	0.103	0.411	0.25	0.211	0.717	0.29	0.114	6.12	0.02
Er (0.10 ppm)	0.313	1.25	0.25	0.571	1.91	0.30	0.346	18.80	0.02
Tm (0.03 ppm)	0.049	0.192	0.25	0.083	0.258	0.32	0.055	2.77	0.02
Yb (0.10 ppm)	0.306	1.30	0.23	0.541	1.58	0.34	0.368	18.80	0.02
Lu (0.01 ppm)	0.049	0.208	0.23	0.078	0.225	0.35	0.063	3.01	0.02
ΣREE	8	65	-	23	161	-	41	1410	-

https://doi.org/10.1017/S0954102006000411 Published online by Cambridge University Press

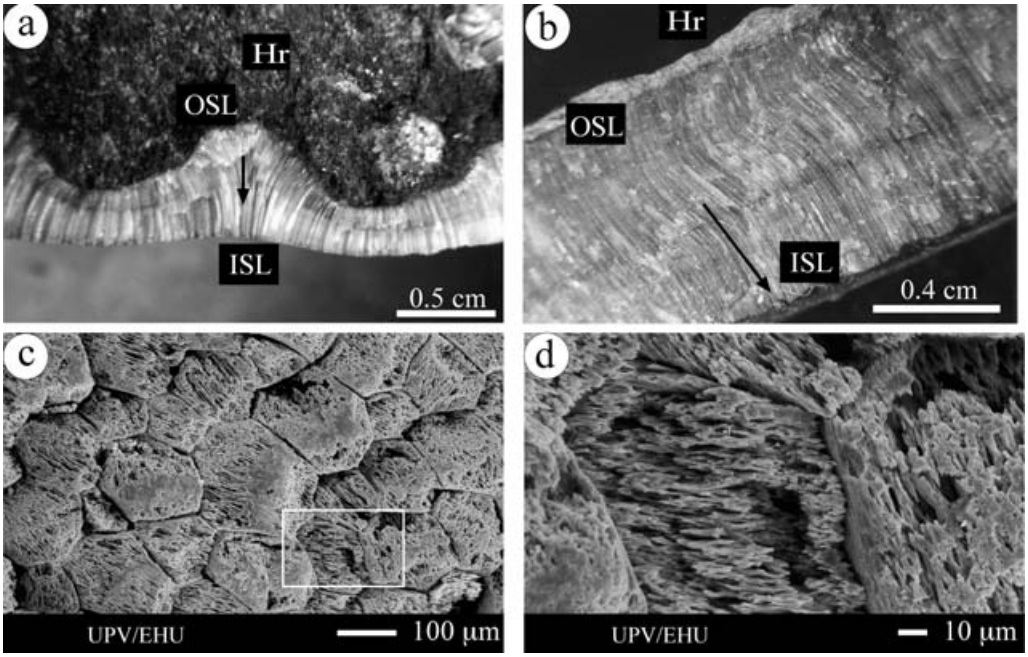

Fig. 3. Inoceramid specimens at the lower Campanian strata of the James Ross Basin (Antarctica). **a.** Hand sample of *Inoceramus* sp. (sample SM, earliest Campanian) showing a fan-like arrangement of calcite prisms. **b.** Hand sample of prismatic shell structure of *A. rabotensis* formed by subparallel, long, and slender calcite prisms. In both cases (a & b), the prisms grow downwards from the outer shell layer (OSL) to the inner shell layer (ISL), as indicated by the black arrows. The host rock (Hr) consists of volcaniclastic sandstone with carbonate cement. **c.** SEM view of the inoceramid prisms, from the ISL, showing the typical pseudo-hexagonal honeycomb microstructure, partially eroded by differential meteoric dissolution (*Inoceramus* sp. SM). **d.** Close-up of the rectangle area in **c**, where the ultrastructure of the calcite prisms can be observed. Note the different orientation for the thin pseudo-rhombic forms that comprise the interior of adjacent calcite prisms.

et al. (1992) and Olivero & Mussel (1993) and were formally describe by Crame & Luther (1997). These specimens are abundant in certain stratigraphical intervals, consisting of alternating fine sandstone and mudstone beds, representative of storm-dominated settings in the offshore transition zone. Most of these inoceramids showed a preferred orientation of the length of the valves with respect to the inferred direction of waves or currents (Olivero & Mussel 1993, Crame & Luther 1997). The living position of *A. rabotensis* was interpreted as an edgewise-recliner, with the commissure in a sub-vertical position and the thicker, shelf-like anterior part of the shell resting on the bottom (Olivero & Mussel 1993), or as a snow-shoe strategist with the commissure lying sub-horizontal and parallel to the sediment substrate (Crame & Luther 1997). Specimens of the smaller *Inoceramus* sp. are relatively abundant in massive tuffaceous horizons in the lower part of the N Sequence at the Brandy Bay section, which are rich in carbonaceous material (Scasso *et al*. 1991) (Fig. 2). Two varieties of shell structure are clearly distinguishable from the studied inoceramid samples. The shell of *Inoceramus* sp. is characterized by a fan-like growth of calcitic prisms with their general arrangement controlled by associated prominent ribs (Fig. 3a). In comparison, the shell of *A. rabotensis* is smooth and without prominent ribs. Furthermore, calcitic prisms in *A. rabotensis* are slender, flexible and have relatively constant width (Fig. 3b).

Under the microscope, the thick outer layer of both inoceramid groups, formed of low magnesian calcite (LMC), consists of branching, small, rod-type prisms in the outer shell layer that give way to a regular, simple prismatic microstructure, with larger prisms, in the inner shell layer. In SEM images the low-Mg calcite prismatic microstructure of *Inoceramus* sp. exhibits the typical honeycomb pattern (Fig. 3c & d). Moreover, some specimens show evidence of boring traces and organic incrustations on the outer shell layer, as previously reported from inoceramid shells from lower latitudes (Basque–Cantabrian Basin) (Elorza & García-Garmilla 1996, 1998, Gómez-Alday *et al*. 2004, Jiménez-Berrocoso *et al*. 2004). The inner aragonitic nacreous layer, previously described for *A. rabotensis* by Crame & Luther (1997) and for other Antarctic inoceramids by Pirrie & Marshall (1990a), is occasionally preserved in the inner shell layer of the studied *A. rabotensis* specimens. It consists of thin laminated aragonitic tablets, partially fused, alternating with enclosing prismatic thin calcitic sublayers (Fig. 4a–h). The presence of aragonite material in *A. rabotensis* shells has been verified also with XRD analysis.

Under CL, *Inoceramus* sp. calcitic prisms present a bright

https://doi.org/10.1017/S0954102006000411 Published online by Cambridge University Press

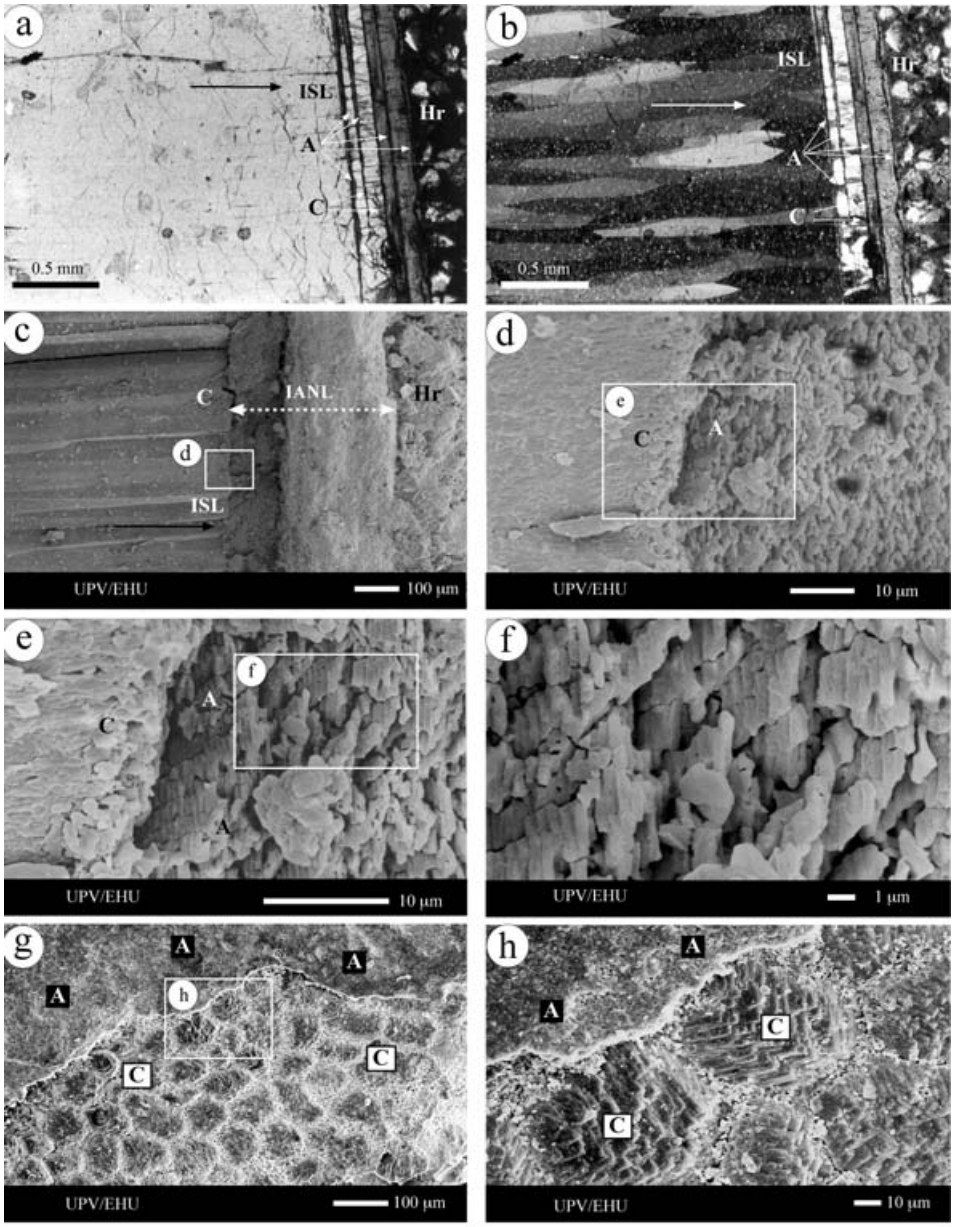

Fig. 4. Shell microstructure of *A. rabotensis* (sample F-71, latest early Campanian). **a.** Plane-light view of a thin-section showing a detail at the ISL, where the low-Mg calcite (LMC) prismatic layer can be differentiated from the inner aragonitic nacreous layer. The latter consists of alternating brownish aragonitic (A) and clear calcitic (C) thin sublayers. Black arrow indicates the direction of prism growth. **b.** The same area as **a** under cross-polars. Note the clear distinction between aragonitic and calcitic sublayers, with no evidence of neomorphism. **c.** Inoceramid view similar to **a** & **b** under SEM. It can be observed the contact of the LMC prismatic layer (C), at the ISL, with the inner aragonitic nacreous layer (IANL), without sublayer distinction. **d–f.** Successive close-ups of the contact between the LMC prismatic layer (C) and the sheet aragonitic structures (A) with weak compaction. **g.** View perpendicular to the prism length axes from the ISL, with the honeycomb microstructure of calcite prisms (C) clearly differentiated from the inner aragonitic nacreous layer (A). **h.** Close-up of the rectangle area in **g**, showing a detail of the contact between the LMC prismatic layer (C) with the inner aragonitic nacreous layer (A).

reddish-yellow colour, clear evidence of diagenetic modification, with the contact between prisms (inter-prismatic zones) showing bright yellowish luminescence (Fig. 5a). Most of the *A. rabotensis* sections, however, present brighter yellowish luminescence close to the boundary of both the outer shell layer and inner shell layer, which gradually gives way to reddish and to non-luminescent zones towards the central part of the shell (Fig. 5b). Within the less luminescent and diagenetically modified zones of *A. rabotensis*, thin dark lines (*laminae obscurae*) are visible as alternating bright yellow lines under CL. A dense grouping of these lines may define

https://doi.org/10.1017/S0954102006000411 Published online by Cambridge University Press

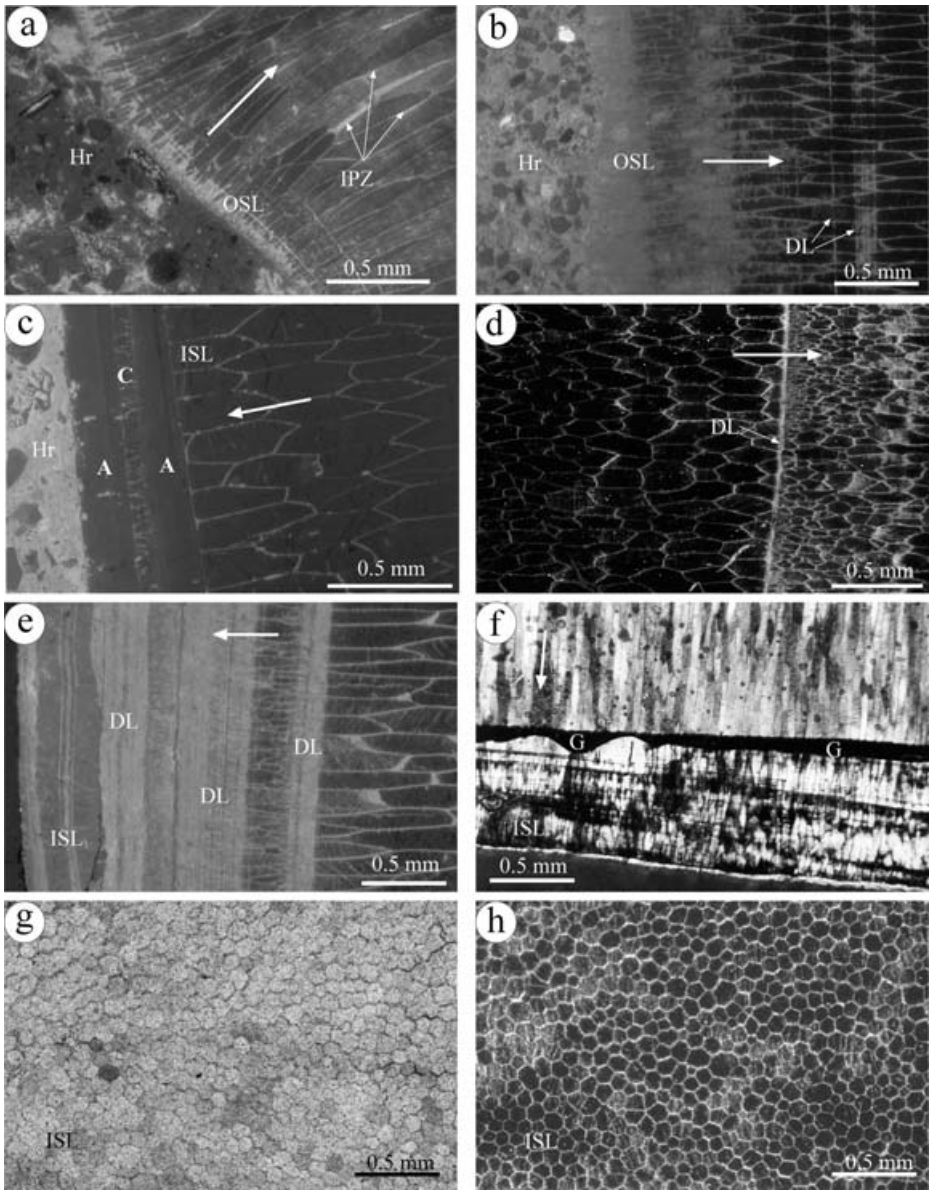

Fig. 5. Shell microstructures of *Inoceramus* sp. (earliest Campanian) and *A. rabotensis* (latest early Campanian) from the James Ross Basin. **a.** LMC prismatic layer of *Inoceramus* sp. (sample SM) under CL, with bright yellowish-red luminescence. A yellowish luminescence characterizes the inter-prismatic zones (IPZ) at the prism boundaries, caused by secondary calcite cements. Note the irregular volcanic grains in the host rock (Hr), most of them non-luminescent, and the luminescent cement. **b.** LMC prismatic layer of *A. rabotensis* (sample Re-b) under CL, showing bright yellowish luminescence at the OSL, which gradually gives way to reddish and to non-luminescent zones towards the central part of the shell. Dark, organic-rich lines (DL) exhibit bright yellowish luminescence. **c.** A detail of the microstructure of *A. rabotensis* (sample F-71) at the ISL under CL. The LMC prismatic layer is differentiated from the inner aragonitic nacreous layer, the latter formed by two reddish luminescent aragonitic (A) sublayers enclosing a thin calcitic (C) sublayer. The host rock (Hr) cement has bright yellow luminescence. **d.** LMC prismatic layer of *A. rabotensis* (sample I3) under CL. A yellow luminescent dark, organic-rich line (DL) marks the interruption of the normal-sized calcite prisms. After that, the smaller and newly formed calcite prisms progressively recover normal size (see main text for interpretation). **e.** Detail of the LMC prismatic microstructure of *A. rabotensis* (sample Re-1T) at the ISL under CL. Note calcite prisms abruptly interrupted by a dense group of dark, organic-rich lines (DL). Smaller prisms initiate their growth after this interruption but they are further interrupted by the presence of denser dark lines and irregular surfaces (see main text for interpretation). **f.** LMC prismatic microstructure of *A. rabotensis* (sample Re-a) at the ISL (cross nicols), showing a glauconite-rich layer (G) that interrupts the normal growth of calcite prisms. The glauconite-rich layer gives way laterally to an organic-rich layer (see main text for interpretation). Thick white arrows indicate the direction of growth of the prisms in all the photographs. **g.** Poorly defined pseudo-hexagonal honeycomb pattern of the ISL under plane-light view (sample 8a, latest early Campanian). **h.** The same area as **g**, under CL, where a honeycomb pattern, with mainly non-luminescent prismatic patches, is well defined. The bright yellowish luminescent thin film of diagenetic calcite is present at the prism boundaries.

https://doi.org/10.1017/S0954102006000411 Published online by Cambridge University Press

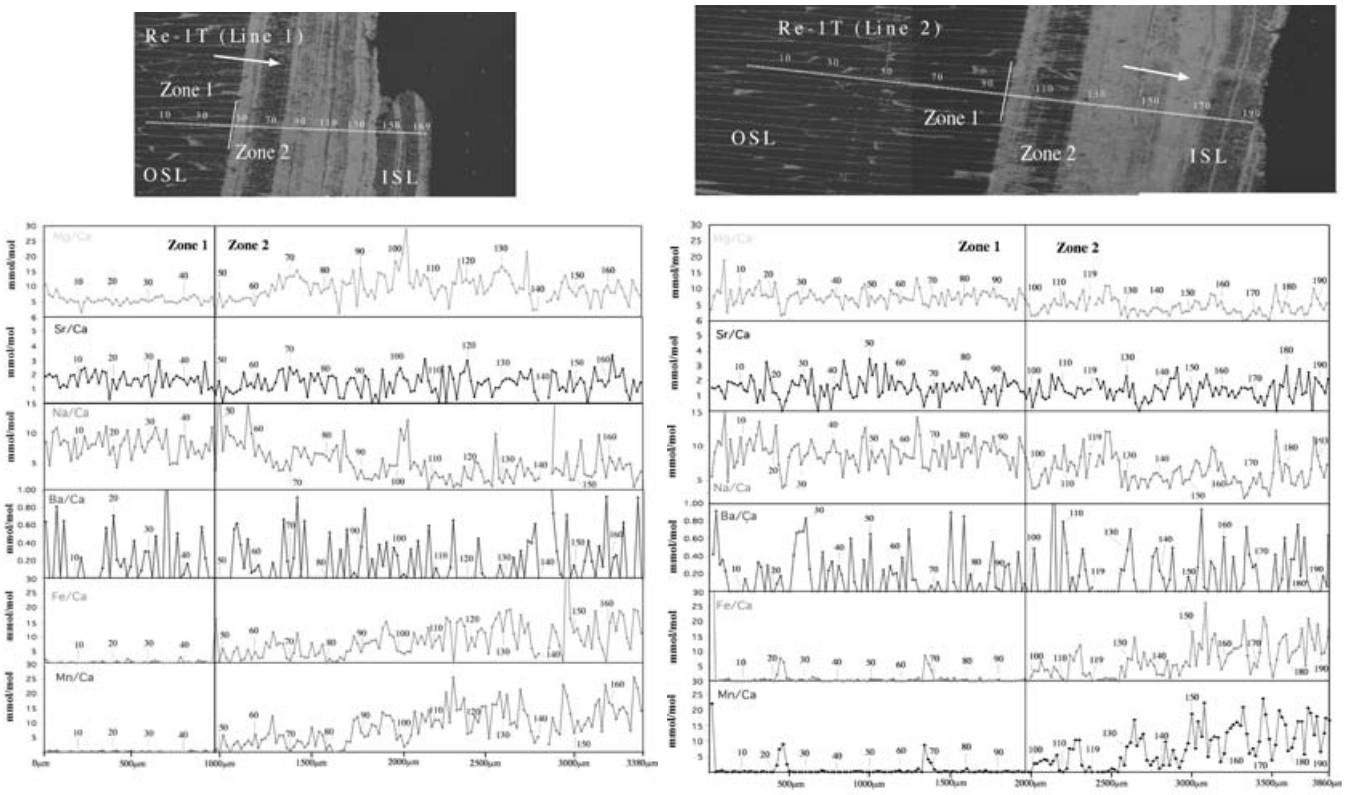

Fig. 6. Thin-section views under CL and MTE profiles (Mg/Ca, Sr/Ca, Na/Ca, Ba/Ca, Mn/Ca and Fe/Ca ratios) for the luminescence-zoned shell Re-1T, with 2 zones differentiated. White arrows indicate the direction of prism growth. Spots represent the microprobe transects (169 for Line 1 and 193 for Line 2). All the elemental ratios exhibit a similar "saw-toothed" pattern, whose intervals are marked by the distance between the analyses (10 to 20 µm apart), and the amplitudes by the concentration (in mmol/mol). Note the considerably different compositional pattern between zone 1 (non-luminescent) and zone 2 (mainly luminescent), with an abrupt rise in Fe/Ca and Mn/Ca contents, starting from spots 49 and 100, respectively.

organic matter-rich layers, alternating with the rest of the prism material (*laminae pellucidae*). The inner aragonitic nacreous layer identified in *A. rabotensis* shells, consisting of the afore-mentioned alternating thin aragonitic and calcitic sublayers, exhibits low intensity reddish luminescence with respect to the yellowish luminescence of the calcitic cement in the host rocks (Fig. 5c). Particularly distinguishable under CL is the anomalous microstructure of the shell layering in the low-Mg calcite prismatic layer of *A. rabotensis*, also detected by Elorza *et al*. (2001), which is dealt with below (Fig. 5d–f). The typical regular honeycomb microstructure is not well observed under plane polarised light but is perfectly visible under CL, where luminescence is mainly restricted to the inter-prismatic zones (Fig. 5g & h).

Geochemical results

Geochemical intra-shell variations throughout the A. rabotensis *microstructure*

By means of EPMA, four geochemical transects have been performed in the most representative *A. rabotensis* thin sections (Re-1T and F-71). Transects in the Re-1T specimen ($\delta^{18}O$ = -4.09‰ PDB; whole-shell from Elorza *et al.* 2001), with 169 (Line 1) and 193 (Line 2) analysed spots respectively, can be divided into two zones, following the geochemical changes together with luminescent behaviour of the shell (Fig. 6a & b). Geochemical transects in Zone 1, extending across nearly the entire analysed inoceramid thin section, cross non-luminescent, well-developed prisms. Moreover, Zone 1 is characterized by yellowish luminescence at both the inter-prismatic zones and the mechanical twins of the prisms; the latter can be used as strain gauges to determine deformation in marine carbonate rocks according to González-Casado *et al*. (2003). Geochemical transects in Zone 2 cross the latest growth stages of this specimen, where the prisms are smaller as a consequence of clear interruptions in the growth of the microstructure. Accordingly, it exhibits an alternation of dense, thin dark and light growth lines up to the very margin of the shell (inner shell layer), where the inner aragonitic nacreous layer cannot be distinctly observed.

Transects in *A. rabotensis* F-71 ($\delta^{18}O$ = -4.32‰ PDB; whole-shell from Elorza *et al.* 2001) include two lines of 169 (Line 1) and 136 (Line 2) analysed spots, respectively (Fig. 7a & b). The external-most part of the outer shell layer

https://doi.org/10.1017/S0954102006000411 Published online by Cambridge University Press

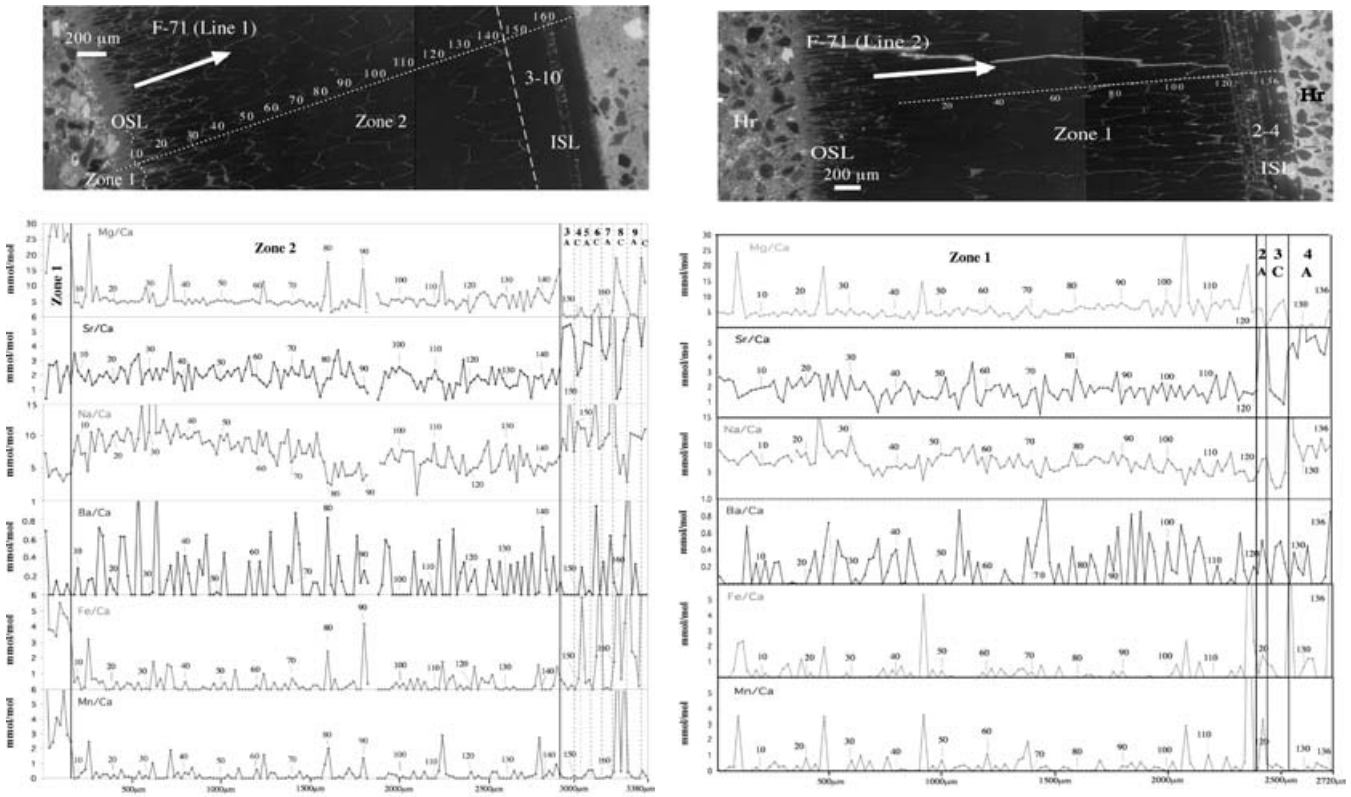

Fig. 7. Thin-section views under CL and MTE profiles (Mg/Ca, Sr/Ca, Na/Ca, Ba/Ca, Mn/Ca and Fe/Ca ratios) for shell F-71. Spots represent the microprobe transects (169 for Line 1 and 136 for Line 2, with 10 and 4 zones differentiated, respectively). All the elemental ratios exhibit a "saw-toothed" pattern, whose intervals are marked by the distance between the analyses (10 to 20 µm apart), and the amplitudes by the concentration (in mmol/mol). White arrows indicate the direction of growth of the prisms. Note how Line 1 presents visible compositional differences between the small zone 1 (luminescent) and the greater part of zone 2 (non-luminescent). The inner aragonitic nacreous layer, starting at the spot 146 in Line 1, has been differentiated into 8 zones, with calcite (zones 4, 6, 8 and 10) and aragonite (zones 3, 5, 7 and 9). The weak diagenetic alteration at the ISL permits the establishment of compositional differences. The same behaviour is visible in Line 2, where the inner aragonitic nacreous layer starts at the spot 121, but with a minor number of calcitic (zone 3) and aragonitic (zones 2 and 4) areas. Diagenetically altered analyses, precisely in the inter-prismatic zones, coincide with pronounced troughs in both profiles and have been segregated of necessity (see Table I and Fig. 8).

in F-71 (Zone 1 of Line 1), with smaller prisms, is distinctly luminescent with respect to the rest of the inoceramid thin section (Zone 2 of Line 1; Zone 1 of Line 2). Importantly, the occurrence of an original alternation of aragonitic and calcitic sublayers (inner aragonitic nacreous layer) is clearly shown in the inner shell layer of F-71. Both the alternating luminescent behaviour of the shell and geochemical variations detected by the microprobe transects in the ISL have permitted the differentiation of up to four aragonite-calcite couplets, especially for Line 1. Thus, eight subzones for Line 1 (Zone 3 to 10) and three for Line 2 (Zone 2 to 4) have been differentiated along the geochemical transects in the inner shell layer of F-71 (Fig. 7a & b). In addition, a few of the analysed spots in shells Re-1T and F-71 are located in the luminescent inter-prismatic zones, which have been separated from the rest of the geochemical analyses.

The minor and trace element (MTE) contents detected by EPMA in the differentiated zones of *A. rabotensis* shells (Re-1T and F-71) are reported in millimoles of each cation relative to moles of Ca^{2+} (mmol/mol) (Table I). It is noteworthy that all the elemental ratios exhibit "saw-toothed" patterns (Figs 6 & 7), as recently described by Jiménez-Berrocoso *et al*. (2004) in Santonian inoceramid shells from the Basque–Cantabrian Basin. The Mg/Ca ratios of *A. rabotensis* Re-1T and F-71 have distinctly higher mean values in the luminescent low-Mg calcite prismatic zones (more diagenetically altered) (Fig. 8). In the non-luminescent prismatic zones (less diagenetically affected), however, Mg/Ca ratios present more regular "saw-toothed" patterns and lower mean values. These geochemical trends are the opposite of those observed in the Basque–Cantabrian Basin inoceramids, where non-luminescent and less altered prisms were higher in Mg/Ca (Gómez-Alday & Elorza 2003, Jiménez-Berrocoso *et al*. 2004). The thin originally aragonitic sublayers detected in specimen F-71 are clearly depleted in Mg/Ca (Zones 3, 5, 7 and 9 of Line 1; Zones 2 and 4 of Line 2), with respect to the enclosing calcitic sublayers (Zones 4, 6, 8 and 10 of Line 1;

https://doi.org/10.1017/S0954102006000411 Published online by Cambridge University Press

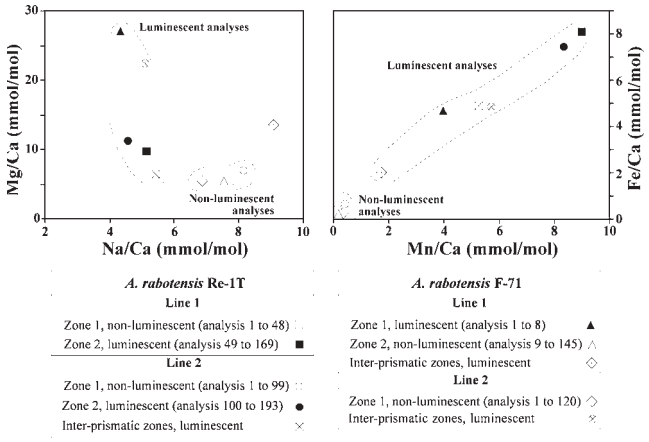

Fig. 8. Diagrams showing the MTE contents (mmol/mol) from Table I for the non-luminescent, luminescent and inter-prismatic analyses obtained from the microprobe transect on *A. rabotensis* Re-1T (Lines 1 and 2) and F-71 (Lines 1 and 2). The relationships of Mg/Ca *vs*. Na/Ca, and Fe/Ca *vs*. Mn/Ca are shown. Different areas, marked by dashed lines, indicate that luminescent and inter-prismatic analyses (more diagenetically altered) are mainly enriched in Mg/Ca, Fe/Ca and Mn/Ca with respect to the non-luminescent analyses (less diagenetically affected), which are, in contrast, enriched in Na/Ca.

Zone 3 of Line 2) (Fig. 9). This finding confirms that the existence of the inner aragonitic nacreous layer of *A. rabotensis* can be identified both with petrographic techniques (Elorza *et al*. 2001) and with microprobe transects. Furthermore, it is evident that the inner aragonitic

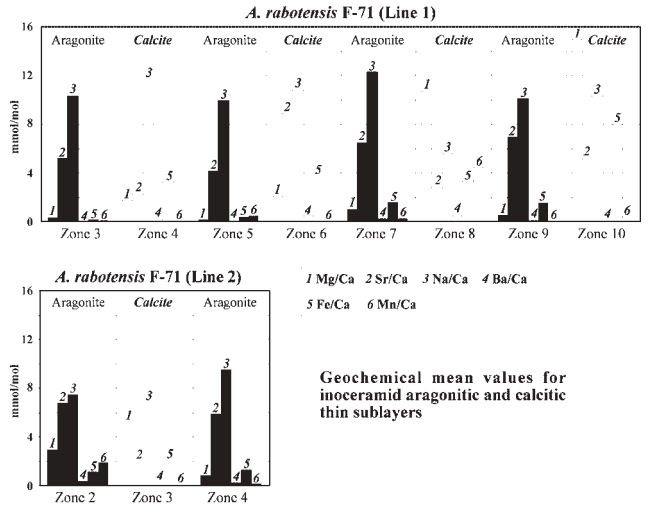

Fig. 9. Histograms showing the geochemical mean values (mmol/mol) for the alternating aragonitic and calcitic thin sublayers (differentiated by zones) that form the inner aragonitic nacreous layer of *A. rabotensis* F-71 (microprobe transects of Lines 1 and 2) (see Table I for the mean values). On a general basis, an increase in Sr/Ca and Na/Ca is observed in the aragonite zones, whereas Mg/Ca, Fe/Ca and Mn/Ca are usually higher in the calcite zones.

nacreous layer of the analysed specimens was originally formed by alternating thin calcitic and aragonitic sublayers. Sr/Ca ratio mean values of Re-1T and F-71 are quite similar both in the luminescent and non-luminescent prismatic zones. In the aragonitic sublayers of F-71, however, Sr/Ca ratios appear distinctly enriched relative to the thin calcitic sublayers (Fig. 9).

Na/Ca profiles all exhibit wave-like trends along the transects of Re-1T and F-71, with the mean values notably higher in the non-luminescent prismatic zones (Fig. 8). Although not as evident as in the former elemental ratios, Na/Ca mean values of F-71 are slightly higher in the aragonitic sublayers than in the calcitic ones (Fig. 9). In contrast, Ba/Ca profiles present characteristic "saw-toothed" patterns, with many prominent and cuspated values. Furthermore, luminescent and non-luminescent prismatic zones of Re-1T and F-71 have low and similar

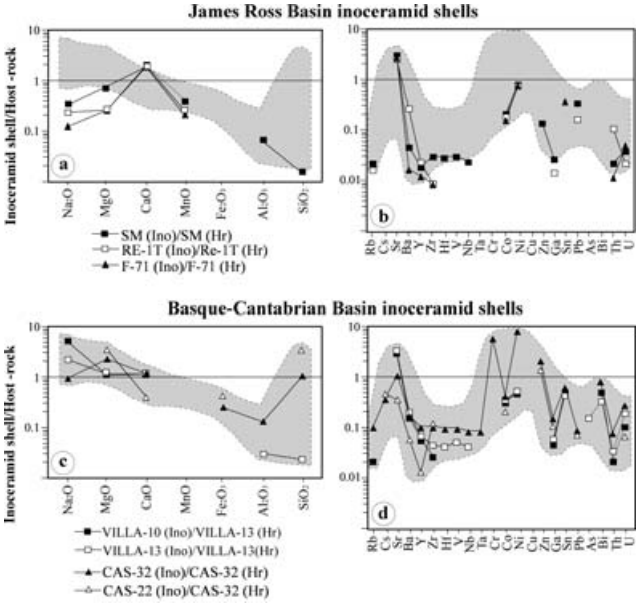

Fig. 10. Diagrams showing the whole-sample geochemistry of inoceramid shells (Ino) and host rocks (Hr) (see Table II for whole-sample values). **a.** & **b.** Data from the James Ross Basin inoceramids: *Inoceramus* sp. (sample SM) and *A. rabotensis* (samples Re-1T and F-71). **c.** & **d.** Data from the Basque-Cantabrian Basin inoceramids (uppermost late Coniacian-lower Santonian): shell samples VILLA-10 and VILLA-13 from the Villamartín section, and CAS-22 and CAS-32 from the Isla de Castro section (Jiménez-Berrocoso 2004). In all the graphs, data represent inoceramid values relative to that of their respective host rocks. The value of the host rock corresponds to unity. Results from the Basque-Cantabrian Basin shells reveal a general pattern of geochemical behaviour for these inoceramids. This pattern is represented by a greyish dashed area and can be used as a reference element for comparison. It can be seen that most geochemical elements present a similar pattern of variation for the inoceramids of the same basin, although the pattern is distinct between shells from different basins.

https://doi.org/10.1017/S0954102006000411 Published online by Cambridge University Press

Ba/Ca mean values. In the F-71 shell, Ba/Ca mean values are very low for the aragonitic sublayers, whereas they are slightly higher for the calcitic ones.

Fe/Ca and Mn/Ca "saw-toothed" profiles both present similar trends in the *A. rabotensis* shells. Their mean values are clearly enriched in the luminescent prismatic zones with respect to the non-luminescent ones (Fig. 8). Moreover, in shell F-71, Fe/Ca and Mn/Ca mean values are distinctly higher for the calcitic sublayers, whereas they are generally depleted and under analytical detection limits in the aragonitic ones (Fig. 9).

Finally, analyses in the luminescent inter-prismatic zones, differentiated from the rest of the microprobe spots, show a similar geochemical behaviour to that of the (intra-) prismatic luminescent zones (Zones 2 of Re-1T; Zone 1 of F-71). In Re-1T (Line 2) and F-71 (Lines 1 and 2), luminescent inter-prismatic zones are mainly enriched in Fe/Ca, Mn/Ca and Mg/Ca mean values, relative to the non-luminescent prismatic ones (Fig. 8). In contrast, Sr/Ca and Na/Ca mean values are generally depleted in the luminescent inter-prismatic zones with respect to the non-luminescent prismatic ones. Ba/Ca ratios show an ambiguous pattern.

Whole-sample (inoceramid shell and host rock) geochemical composition

Three inoceramid whole-shell samples (*A. rabotensis* Re-1T and F-71; *Inoceramus* sp. SM) and their respective host rocks have been analysed for their major, minor and trace element content, including REE (Tables II & III). We have compared the geochemical contents of each inoceramid whole-shell to that of its host rock. Thus, the geochemical concentration of the host rock is represented by unity in every case. On the whole, the concentration of Na_2O, MgO, MnO, Al_2O_3 and SiO_2 in the analysed inoceramids is less than unity (host rock value) (Fig. 10a-b). However, Fe_2O_3 contents are under the analytical detection limits, although CaO and Sr are always above unity in all the shells. Other elements in the shells, such as Rb, Ba, Y, Zr, Co, Zn, Ga, Pb, Th and U, clearly present lower concentrations than those in the host rock (unity). Furthermore, Ni and Sn contents in the inoceramids are close to the host rock value. Finally, Cs, Ta, Cr, Cu, As and Bi, with low concentrations in the host rock, appear under analytical detection limits in all the analysed inoceramids (Table II).

Apart from the above geochemical contents, we have found two slightly different geochemical patterns for the three analysed inoceramid whole-shells, revealed by the detection of major and trace elements, such as Al_2O_3, SiO_2, Hf, V and Nb, exclusively in *Inoceramus* sp. SM, with respect to *A. rabotensis* Re-1T and F-71. Furthermore, the ΣREE of the inoceramids (SM = 41 ppm; Re-1T = 23 ppm; F-71 = 8 ppm) are also symptomatic. In spite of the very low contents relative to the ΣREE host rock values (SM = 1410 ppm; Re-1T = 161 ppm; F-71= 65 ppm) (Table III), *Inoceramus* sp. SM clearly shows a differentiated REE signature with respect to that of *A. rabotensis* Re-1T and F-71 (Fig. 11).

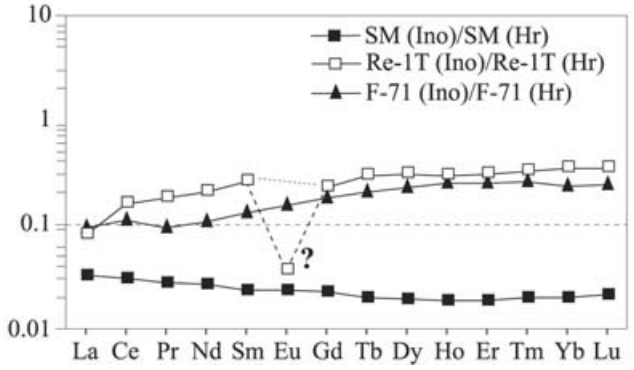

Fig. 11. Graph showing the inoceramid shell (Ino) (*Inoceramus* sp. SM and *A. rabotensis* Re-1T and F-71) REE signatures (see Table III for values). Data represent inoceramid values relative to that of their respective host rocks (Hr). The high Eu value (6.6 ppm) from Re-1T (Hr) probably corresponds to an artefact.

Our geochemical study on inoceramid whole shells has been complemented by comparing it with geochemical data provided by low-latitude inoceramid whole-shells located in different tectono-sedimentary domains of the Basque-Cantabrian Basin (northern Spain). For this purpose, we selected two pairs of inoceramid and host rock, with extreme depleted and enriched oxygen isotope values, from the uppermost Coniacian-lower Santonian Villamartín (VILLA-10; $\delta^{18}O$ = -2.32‰ PDB and VILLA-13; $\delta^{18}O$ = -4.60‰ PDB) and Isla de Castro (CAS-32; $\delta^{18}O$ = -2.05‰ PDB and CAS-22; $\delta^{18}O$ = -4.51‰ PDB) successions (Jiménez-Berrocoso 2004). The comparison of these data reveals two different geochemical patterns in the two groups of inoceramid whole-shells (James Ross Basin vs Basque-Cantabrian Basin), characterized, respectively, by different major and trace elements in the two groups (Fig. 10a–d).

Discussion

Textural features of diagenesis in A. rabotensis

Elorza *et al*. (2001) reported different degrees of diagenetic modification in the Campanian inoceramids from the James Ross Basin. Diagenesis was mainly detected by both the depleted stable isotope values ($\delta^{18}O$ = -4.32 to -3.01‰ PDB) and the CL emission of the shells collected from the Brandy Bay, Santa Marta and Redonda Point sections. In the present work, we have confirmed that the prismatic microstructure of *Inoceramus* sp. (earliest Campanian) shows a bright reddish luminescence, indicative of a more intense diagenetic alteration than *A. rabotensis* (Fig. 5a). In addition, we have found that *A. rabotensis* (latest early Campanian) has a yellowish luminescent emission near the

https://doi.org/10.1017/S0954102006000411 Published online by Cambridge University Press

boundary of both outer shell layer and inner shell layer, with the central part of the shells almost completely non-luminescent (Fig. 5b). Furthermore, the inter-prismatic zones and dark growth lines are always luminescent in the two geochemically analysed inoceramid species. These facts are all indicative of an apparently selective diagenetic modification in the shells, especially for *A. rabotensis*. In this regard, diagenetic alteration in *A. rabotensis* was principally restricted to the margin of the shells (outer shell layer and inner shell layer) and to the inter-prismatic zones, where the low-Mg calcite prismatic microstructure was just in contact with diagenetic pore-fluids. Likewise, Elorza & García-Garmilla (1996, 1998) found similar selective diagenetic alteration in some inoceramid shells from the Santonian and Maastrichtian rocks of the Basque Arc domain (northern Spain). A yellowish-red luminescence characterized the outer shell layer-inner shell layer and inter-prismatic zones of these shells, evidence of localized geochemical replacement during burial diagenesis.

Taking into account the depleted oxygen isotope values of *A. rabotensis* Re-1T and F-71, -4.09 and -4.32‰ PDB respectively (Elorza *et al*. 2001), the occurrence of a presumably homogeneous intense diagenetic alteration throughout the low-Mg calcite prismatic microstructure would be expected. This is, however, in disagreement with the above CL inferences of restricted diagenetic modification in *A. rabotensis*. Apart from diagenesis that possibly modified the primary isotopic composition of the shells, other factors acting during the inoceramids' lifespan could have promoted originally depleted oxygen isotope values (Elorza *et al*. 2001). Likely factors could include:

a) contrasting segregation of shell material during warmer (*laminae pellucidae*) and colder (*laminae obscurae*) periods (Harrington 1986, Clarke 1990),

b) shell growth in waters relatively enriched in ^{16}O during decomposition of volcaniclastic materials to smectite and mixed-layer clays (Lawrence *et al*. 1979, Whittaker *et al*. 1987, Pirrie & Marshall 1990a) and/or

c) a supply of continental fresh-water depleting surface waters with respect to $\delta^{18}O$ in a semi-enclosed warm depositional basin (Price & Sellwood 1997).

Geochemical features of diagenesis in A. rabotensis

Minor and trace element analyses along the transects of Re-1T and F-71 further support the notion of limited diagenesis in *A. rabotensis*. Minor and trace element intra-shell variations indicate a strong relationship between the geochemistry of the shells and their restricted luminescence (Figs 6 & 7; Table I). It is generally accepted that CL in carbonates results from the content in activating cations (e.g. Mn^{2+}), counteracted by the existence of other quenching elements such as Fe^{2+} (Machel 1985, 2000). These cations have long been used as diagenetic indicators due to their frequent increase with burial diagenesis (Brand & Veizer 1980, Al-Asm & Veizer 1982, Brand & Morrison, 1987). Considering the most luminescent zones differentiated in the low-Mg calcite prismatic microstructure of Re-1T (Zone 2 of Line 1 and Line 2) and F-71 (Zone 1 of Line 1), we have found an expected Fe/Ca and Mn/Ca increase (Fig. 8), evidence of cationic substitution in such luminescent zones. Interestingly, Mg/Ca ratios seem to be directly related to Fe/Ca and Mn/Ca, since they (Mg/Ca) usually present higher values in the same luminescent prismatic zones. This fact suggests that Fe^{2+}, Mn^{2+} and Mg^{2+} incorporation was controlled by the same, either primary or diagenetic, factors. As mentioned above, rather than being primary controlled, enrichments in Fe^{2+} and Mn^{2+} are thought to be diagenetic in origin and therefore Mg^{2+} enrichment could be diagenetic as well. Accordingly, diagenetic incorporation of Mg^{2+} into *A. rabotensis* could have been partially related to increased levels of dissolved Mg^{2+} in pore-fluids, a likely consequence of the decomposition of volcaniclastic materials to Mg-rich clays [e.g. smectite, (Al, Mg) $(OH)_2$ Si_4O_{10} Na $(H_2O)_4$] during burial (Lawrence *et al*. 1979, Whittaker *et al*. 1987, Pirrie & Marshall 1990a). In contrast, however, previous studies on Basque-Cantabrian Basin inoceramids detected high contents of original Mg^{2+} incorporated in the shells (Gómez-Alday 2002, Gómez-Alday & Elorza 2003, Jiménez-Berrocoso 2004, Jiménez-Berrocoso *et al*. 2004). In this regard, we cannot discard the notion that diagenetic enrichments of Mg^{2+} in the luminescent prismatic zones of *A. rabotensis* could have been a secondary supplement to originally high contents of Mg^{2+} in the whole-shells. This hypothesis is further supported by the occurrence of Mg^{2+} as the minor and trace element with the highest content in the studied shells (Table I), apart from Ca^{2+}, which is evidence of a significant concentration of Mg^{2+} in the low-Mg calcite prisms prior to diagenesis.

The intra-shell variations of other ratios, such as Sr/Ca and Na/Ca, can also be correlated with the luminescent behaviour of the shells (Figs 6 & 7; Table I). Higher mean values of these cations in the less luminescent zones of Re-1T (Zone 1 of Line 1 and Line 2) and F-71 (Zone 2 of Lines 1 and 2), especially for Na^+ (Fig. 8), indicate less effective cationic exchanges with pore-fluids during burial. Consequently, the less luminescent prismatic zones of *A. rabotensis* shells are expected to have undergone weak diagenetic modification and part of the original geochemical intra-shell variations, particularly those for Sr/Ca and Na/Ca, may preserve primary variation. As regards Ba/Ca ratios, their detected ambiguous pattern, without a clear connection with the luminescence of the shells, also suggests partial preservation of the primary intra-shell variations along the *A. rabotensis* sections.

The whole-shell geochemistry can provide important clues as to the diagenetic alteration of the analysed

https://doi.org/10.1017/S0954102006000411 Published online by Cambridge University Press

inoceramids. Particularly indicative are the REE contents of carbonate materials (McLennan 1989), because diagenetically altered inorganic and biogenic materials (carbonate and apatite) present increased levels of REE (Wang *et al*. 1986, Banner *et al*. 1988, Qing & Mountjoy 1994) compared to those originally preserved (Saw & Wasserburg 1985, Palmer 1985, Reynard *et al*. 1999, Lécuyer *et al*. 2003, 2004). The analysed inoceramid whole-shells (Re-1T, F-71 and SM) all show lower REE contents than their host whole rocks (Fig. 11), the latter being the main sources for REE during diagenesis (Banner *et al*. 1988, Grandjean & Albarède 1989, McLennan 1989, Qing & Mountjoy 1994, Haley *et al*. 2004). This fact indicates that diagenetic incorporation of REE into the shells was not so relevant as to significantly elevate their primary low contents. In accordance with previous inferences from CL and minor and trace element data, the REE results confirm a weak diagenetic alteration in the shells, especially in *A. rabotensis* Re-1T and F-71.

Considering the above interpretation, it is further suggested that diagenetic modification in the whole-shells, and thus their geochemistry (major, minor and trace elements), was importantly influenced by the geochemical nature of their host rock. The most relevant evidence of that is found by comparing data from the James Ross Basin shells with those from the Basque-Cantabrian Basin inoceramids (Fig. 10a–d). Host rocks from the Brandy Bay and Redonda Point sections (James Ross Basin) bear important volcaniclastic components, which make them quite different from the carbonate-rich facies rocks of the Basque-Cantabrian Basin sections. The comparison of the data indicates that most geochemical elements show a similar pattern of variation for inoceramids from the same basin, although this pattern is clearly different between shells from different basins. A likely explanation for these facts can be found in that the host rock was able to modify, in a different way for each basin, the availability of cations in pore-fluids through the different diagenetic transformations of their main components (e.g. volcanic grains and clays).

Palaeoenvironmental stress in A. rabotensis *low-Mg calcite prismatic microstructure*

It is well known that shell accretion in bivalve molluscs takes place by adding shell material in periodic growth increments. These increments are represented by alternating light, inorganic-rich (*laminae pellucidae*) and dark, organic-rich (*laminae obscurae*) growth lines, which reflect the cyclic deposition/dissolution of varying amounts of $CaCO_3$, controlled by the environment and the biological-clock mechanism in the organism. Alternating light and dark growth lines, representing continuous and cyclic increments of still unknown periods, are clearly distinguishable in the studied inoceramid shells (*Inoceramus* sp. and *A. rabotensis*). However, only the *A. rabotensis* shell microstructure (Re-1T and F-71) presents marked growth breaks (Fig. 5d–f), interpreted by Elorza *et al*. (2001) as reflecting conditions of strong palaeoenvironmental stress, based on their analogy with the detailed information provided by extant shallow-water bivalves (Kennish 1980). Diagenetic modifications are unlikely to have caused such microstructural features in the analysed *A. rabotensis* shells, since CL and minor and trace element data, along with whole-shell geochemistry, all indicate weak diagenesis. Furthermore, the absence of neomorphism in the inner aragonitic nacreous layer supports the notion that the marked growth breaks are primary characteristics (Fig. 4a–h). The observed reddish luminescence in this layer, although somewhat indicative of diagenetic alteration, does not imply that such alteration was so critical as to produce the polymorphic transformation from aragonite to calcite in the case of the aragonitic sublayers (Fig. 5c). Moreover, we consider the calcitic sublayers as prevented from any type of recrystallization since they exhibit good textural preservation, similar to that found in the low-Mg calcite prisms. The most characteristic features of growth breaks, mentioned by Elorza *et al*. (2001), in the *A. rabotensis* shells are:

(a) Abrupt growth interruption of normal-sized calcitic prisms (*laminae pellucidae*), marked by a thin, dark organic-rich line (*laminae obscurae*) followed by renewed growth of markedly smaller calcitic prisms (Fig. 5d). This marked break is interpreted to be a result of substantial cooling, temporarily interrupting normal shell growth, reflected by the deposition of an organic-rich line. Subsequently, the growth of initial small-sized calcitic prisms, grading to normal size in the direction of shell growth, would follow the gradual recovery of seawater temperature.

The interruption of continuous shell growth by the abrupt appearance of a dark, organic-rich line may be interpreted following the ideas of Lutz & Rhoads (1977). The active filtration of well-oxygenated waters results in the deposition of $CaCO_3$-rich material, along with diluted organic material (*laminae pellucidae*), when the organism exhibits an aerobic metabolism. As the dissolved oxygen concentration falls in the internal microenvironment of a bivalve during shell closure, anaerobic respiration results in a rise of acidic end products (succinic acid; $COOH\text{-}CH_2\text{-}CH_2\text{-}COOH$) in the extrapallial fluid. The acid build-up is neutralized by the dissolution of shell $CaCO_3$. This decalcification process increases the ratio of acid-insoluble organic material to $CaCO_3$ at the shell-mantle interface. Upon re-opening of the valves, with the consequent continuation of aerobic metabolism, deposition of $CaCO_3$ and organic material within a region containing an abundance of insoluble organic residue should result in a localized increase in the ratio of organic material to $CaCO_3$. The end product of this

https://doi.org/10.1017/S0954102006000411 Published online by Cambridge University Press

process is an organic-rich growth increment (*laminae obscurae*). When a dark, organic-rich line (*laminae obscurae*) of inoceramid shells did not mark the interruption in the size of calcitic prisms, the situation is interpreted in terms of normal seawater palaeotemperature changes, presumably driven by cyclic seasonal processes. In that case, it could be suggested that temperature drop was not so intense as to produce a marked change in the calcitic prism size after depositing the dark, organic-rich line.

(b) Abrupt growth interruption of normal-sized calcitic prisms (*laminae pellucidae*), in the inner shell layer, caused by thick, organic-rich lines (*laminae obscurae*) with alternating dissolution surfaces (Fig. 5e). Under CL, a delicate pattern of dozens of thin yellow organic-rich lines alternating with red organic-poor lines is distinctly observable (Re-1T). This finding is considered as indicative of a continued trend of changes in the segregation of calcite material by the organism, probably promoted by fall and recovery temperatures with a strong seasonal stress in bottom seawater. The alternating pattern and thickness of these lines are in contrast with the general disposition of the fewer dark lamina along both the outer shell layer and the central part of the shell.

(c) Truncation of normal-sized calcitic prisms by a laminar, glauconite-rich layer (Fig. 5f). This layer is irregular in thickness, with a curved surface at the top, and finishes laterally as a thin, organic-rich surface between calcitic prisms. In the opinion of Elorza *et al*. (2001), this is an anomalous microstructural modification of inoceramid shells that is difficult to account for. Selective replacement by glauconite is known in various types of organisms, including inoceramid shells (Nockolds *et al*. 1979, Haggart & Bustin 1999), but they always seem to be post-mortem replacements. In our case, a coherent explanation for *in-vivo* replacement could be an abrupt halt in normal prismatic shell growth. The necessary ions for glauconite formation would be expelled from underlying glauconite-rich pore-fluids of sandy-silty sediments to the bottom seawater.

We have confirmed that the marked growth breaks in the shell microstructure of *A. rabotensis* are restricted to the specimens recorded in the stratigraphical levels just below the earliest late Campanian disappearance event of the James Ross Basin inoceramids. Therefore, the microstructural growth breaks seem to mark a strong change in the palaeoenvironmental conditions, preceding and finally leading to the early disappearance of the group in the James Ross Basin (Crame *et al*. 1996, Crame & Luther 1997, Elorza *et al*. 2001).

Palaeoenvironmental insights from A. rabotensis *inner aragonitic nacreous layer*

Two relevant features are symptomatic of the inner aragonitic nacreous layer in the inner shell layer of the studied inoceramid shells. First, as described above, it is formed of alternating aragonitic and calcitic thin sublayers (Figs 4a–h, 5c). Second, it shows good textural preservation in the analysed shells, highlighting its usefulness for subsequent palaeoenvironmental interpretations based on geochemical data. Thus, we suggest that the particular alternation of aragonitic and calcitic sublayers in the inoceramid shells could also be a likely product of palaeoenvironmental stress.

A review of the literature on the inner aragonitic nacreous layer of high latitude inoceramids indicates a nearly complete aragonitic composition, with no evidence of originally enclosing calcitic sublayers (Pirrie & Marshall 1990a, Crame & Luther 1997). In low-latitude shells, however, most authors have found no evidence of the inner aragonitic nacreous layer, either original or neomorphed (Elorza & García-Garmilla 1996, 1998, Elorza *et al*. 1997, Gómez-Alday & Elorza 2003, Gómez-Alday *et al*. 2004, Jiménez-Berrocoso *et al*. 2004). Hence, a reasonable explanation for the distinct occurrence of alternating aragonitic and calcitic sublayers can be found in that marked changes in the palaeoenvironmental conditions, just prior to the early disappearance of inoceramids in Antarctica (basal late Campanian), could also have made *A. rabotensis* specimens unable to deposit the inner aragonitic nacreous layer as a whole. In accordance with this, we propose that the latest growth stages of *A. rabotensis* shells underwent continuous changes in the segregation of shell material, between calcite and aragonite, probably encouraged by strong palaeoenvironmental instability in the bottom seawater conditions. In our opinion, it is still premature to hypothesize on the primary palaeoenvironmental factor(s) (e.g. marked temperature changes, food availability, scarcity of appropriate dissolved ions in seawater) responsible for changes in the deposition of the aragonitic and calcitic thin sublayers since we lack other presumably important data (e.g. fine-resolution $\delta^{18}O$ and $\delta^{13}C$ sampling along the shell layering) that would support any proposals.

Nonetheless, clear identification of the alternating aragonitic and calcitic sublayers, by means of the minor and trace element intra-shell variations, provides substantial insights. Geochemical ratios from *A. rabotensis* F-71 show higher Fe/Ca and Mn/Ca, together with Ba/Ca and Mg/Ca, in calcitic sublayers (Zones 4, 6, 8 and 10 of F-71) than in aragonitic ones (Zones 3, 5, 7 and 9) (Figs 7 & 9; Table I). In turn, Sr/Ca and Na/Ca ratios increase in aragonite material with respect to calcite. These findings indicate that geochemical intra-shell variations along the inner aragonitic nacreous layer apparently responded to the mineralogical composition of the analysed sublayers, either aragonite or calcite. This is rather intuitive, considering that the less dense aragonite lattice usually bears higher concentrations of larger cations (e.g. Sr^{2+}, Na^{+}) with respect to the denser

https://doi.org/10.1017/S0954102006000411 Published online by Cambridge University Press

lattice of calcite, in which smaller cations are frequently found in higher amounts. In contrast, in the Basque-Cantabrian Basin inoceramids, Gómez-Alday & Elorza (2003) and Jiménez-Berrocoso *et al*. (2004) interpreted that palaeoenvironmental factors (e.g. cyclic temperature and food availability changes) were the main controls on the geochemical intra-shell variations exclusively along the low-Mg calcite prismatic microstructure. However, our data suggest that the influence of palaeoenvironmental factors on the geochemical intra-shell variations, along the inner aragonitic nacreous layer, was subordinate to that caused by original alternating mineralogical changes (aragonitic and calcitic thin sublayers).

Early disappearance of Inoceramids in Antarctica and aragonite-calcite isotopic palaeotemperatures

The early disappearance of inoceramids in Antarctica was preceded or accompanied by major changes in composition, diversity and biogeographical distribution of early Campanian ammonite fauna from the James Ross Basin (Olivero *et al*. 1999, Olivero & Medina 2000). These relevant faunal changes were accompanied by the exclusion, from southern high latitudes, of several mollusc taxa that are known to have survived up to the Maastrichtian in mid- to low-latitudes elsewhere in the world, including several ammonite (Scaphitidae, Nostoceratidae, Baculitidae and Phylloceratidae), belemnite (Belemnitidae) and bivalve families (Inoceramidae and most of the Trigoniidae) (Olivero 1992, Zinsmeister & Feldmann 1996) (Fig. 2). In particular, Olivero & Medina (2000) found significant changes in the diversity of ammonite fauna from the Campanian–Maastrichtian sedimentary succession of the James Ross Basin. Stratigraphically above a notable regional Maastrichtian unconformity, the MG Sequence (mid-Maastrichtian–Danian) is dominated by the ammonite genera *Maorites* and *Grossouvrites* (Fig. 2), which characterize a marked reduction in the diversity of the molluscan fauna. These diversity patterns are consistent with similar trends observed from microfossils (e.g. planktonic foraminifers) (Huber & Watkins 1992), which could all reflect major palaeoenvironmental controls associated with the marked long-term Campanian-Maastrichtian cooling of southern high latitude oceanic waters (Huber 1998, Huber *et al*. 2002).

On the whole, it is accepted that the particularly adverse conditions preceding the early inoceramid disappearance in the James Ross Basin (10 m.y. before the K/T boundary) progressed slowly towards mid- to low-latitudes, possibly conditioned by tectonic forcing such as the final breaching of Walvis Ridge and Rio Grande Rise (Frank & Arthur 1999). Inoceramid disappearance in deep water palaeoenvironments of the Northern Hemisphere is recorded during the mid-Maastrichtian, just 3.5 m.y. before the K/T boundary in the Gubbio Basin (Italy) and 2.6 m.y. before the K/T in the Basque-Cantabrian Basin (Spain). However, the above-described marked growth breaks, reflecting conditions of palaeoenvironmental stress on *A. rabotensis* shells (Fig. 5d-f), were not recognized in the inoceramid species of the Basque-Cantabrian Basin (Elorza & García-Garmilla 1998). Yet, recent findings have pointed out that the extreme thinness of the inoceramid shells, just prior to their final extinction event in the Basque-Cantabrian Basin, could be one of the causes for not recognizing possible microstructural growth anomalies in the low-Mg calcite prisms (Gómez-Alday 2002, Gómez-Alday *et al*. 2004).

The evolution of the giant size in *A. rabotensis* inoceramid shells was interpreted by Crame & Luther (1997) as a primary antipredatory device. The same authors indicated, however, that just as large predators (e.g. fish and reptiles) were increasingly radiating in the latest Cretaceous, seawater temperatures were falling, thus making the secretion of such a large calcitic shell physiologically impractical. Crame *et al*. (1996) indicated a temperature drop of about 5ºC for bottom seawater in southern high latitudes, from the mid Campanian through the late Maastrichtian. Subsequently, Crame & Luther (1997) stated that this temperature drop could be one of the major factors explaining the afore-mentioned restriction of inoceramids in mid- to low-latitudes, around the margins of the Tethyan Province, during the latest Cretaceous.

Isotopic mean values obtained by Elorza *et al*. (2001) from early Campanian belemnite calcite rostra of the N Sequence (Brandy Bay section, $\delta^{18}O$ = -0.94‰, n = 5; Santa Marta section, $\delta^{18}O$ = -0.50‰, n = 21) were similar to those previously reported by Pirrie & Marshall (1990a, 1990b), Marshall *et al*. (1993), Ditchfield *et al*. (1994) and Crame *et al*. (1996) from well-preserved high latitude macrofossils (belemnites, ammonites, oysters and inoceramids). However, Elorza *et al*. (2001, Fig. 3, Table I) detected that belemnite isotopic values were quite different for distinct samples collected from the same stratigraphic level. The estimated difference was more than 2‰ PDB ($\delta^{18}O$ = 0.94‰ to -1.1‰). Accordingly, these could not be considered as absolute values, since $\delta^{18}O$ palaeotemperature calculations could have been overestimated by a significant supply of fresh water in restricted palaeoenvironments, thus modifying the normal seawater isotopic composition. Despite a possible overestimation in palaeotemperature values, via a surplus of fresh-water supply and diagenetic alteration, there was certainly a marked drop in the seawater palaeotemperature trend provided by belemnites from the late early Campanian (15.8°C) to the mid-/late Maastrichtian (12.5°C). This finding is consistent with the detected, long-lasting climatic cooling for the latest Cretaceous and also supports conditions of palaeo-environmental stress on the studied *A. rabotensis* shells.

Especially significant is the alternative use given to aragonite and calcite material for isotopic

https://doi.org/10.1017/S0954102006000411 Published online by Cambridge University Press

palaeotemperature calculations from inoceramid shells. Most authors have long focused on well-preserved calcitic prisms to obtain feasible $\delta^{18}O$ values from Jurassic and Cretaceous inoceramids (e.g. Schönfeld *et al*. 1991, Ditchfield *et al*. 1994, Hilbrecht *et al*. 1996, Price & Sellwood 1997, Zakharov *et al*. 1999, 2005, Fisher & Arthur 2002, Gómez-Alday *et al*. 2004). In other cases, however, the inner aragonitic nacreous layer was used for isotopic analyses (e.g. Wright 1987, Whittaker *et al*. 1987, Pirrie & Marshall 1990a). Nevertheless, the latter can be even more problematic because the thermodynamic instability of aragonite during diagenesis may produce significant carbonate transformations affecting the original isotopic values. Moreover, given the recognition of a particular inner aragonitic nacreous layer in the studied *A. rabotensis* shells, formed by alternating aragonitic and calcitic thin sublayers (Figs 4a–h, 5c), it would be appropriate to first accurately characterize the carbonate material before analysing for isotopic palaeotemperatures. Consequently, based on the results presented in this paper, we recommend not only carrying out an exhaustive examination for textural and geochemical diagenetic features in the inoceramid carbonate material, but also evaluating the possible mineralogical variability inside the shells, especially in the inner aragonitic nacreous layer. The latter is mostly relevant for selecting a suitable palaeotemperature equation, because mixing carbonate mineralogy can provide rather imprecise results. Furthermore, we consider this work of high importance, especially since new isotopic palaeotemperature data will aid in unravelling the inoceramid bivalve demise from a global perspective.

Several studies have indicated that the final inoceramid biotic crisis lasted about 0.5 m.y. in low-latitudes. The extinction interval does not seem to show any remarkable lithological change, although it is significantly characterized by rapid increases in burrowing organism population, a negative excursion of 0.7‰ in the $\delta^{13}C$ of benthic foraminifers, major decreases in both bi-keeled planktonic foraminifers and inoceramid prism abundance, along with increased ventilation of bottom waters (MacLeod 1994a, 1994b, Chauris *et al*. 1998, Frank & Arthur 1999). Most authors have considered all these factors as evidence of a substantial reorganization of deep-ocean circulation towards cooler and less saline waters, with increased dissolved O_2 levels in the deep-sea (MacLeod & Huber 1996, MacLeod *et al*. 1996). The progressive ventilation of the deep-sea would have led to a decrease in the flux of organic matter (Frank & Arthur 1999), which may also have contributed to the extinction of inoceramid organisms. Moreover, recent data on inoceramid species distribution and stable isotope values from Sopelana sections (Basque–Cantabrian Basin) have provided further evidence of the modification of the marine thermocline and the onset of climatic cooling close to the early/late Maastrichtian boundary as the main causes for the final inoceramid extinction in the Northern Hemisphere (Gómez-Alday *et al*. 2004). In the opinion of these authors, the record of the boreal inoceramid *Spyridoceramus tegulatus*, consistent with a positive $\delta^{18}O$ excursion in the inoceramid extinction interval, suggests the entry of deep, cool and oxygenated waters arriving from the North Atlantic. In deep-sea deposits from Tierra del Fuego, the inoceramid group disappeared during the late Campanian to early Maastrichtian, and the local extinction of the group was accompanied by a marked increase in the degree of bioturbation, which was also related to the incoming of oxygenated bottom waters (Olivero *et al*. 2003, 2004). To sum up, all these features make the diachronous disappearance of inoceramid bivalves, observed first in the basal late Campanian (James Ross Basin) and finishing close to the early/late Maastrichtian boundary (Basque-Cantabrian Basin), an event of attractive worldwide attention, in which, however, much information remains to be debated to completely understand it.

Conclusions

Varying degrees of diagenesis have been demonstrated in Campanian inoceramids from the James Ross Basin (Antarctica). The low-Mg calcite prismatic microstructure of *Inoceramus* sp. (earliest Campanian) exhibits bright reddish-yellow luminescence, indicative of significant diagenetic modification. In contrast, luminescence in *A. rabotensis* specimens (latest early Campanian) is mostly localized both at the margin of the shells and the inter-prismatic zones, which is evidence of diagenetic modification restricted to the contact of the prismatic microstructure with pore-fluids. Good textural preservation of the original inner aragonitic nacreous layer in *A. rabotensis* further indicates weak diagenetic alteration.

Newly obtained minor and trace element intra-shell variations along *A. rabotensis* transects, with a characteristic "saw-toothed" pattern, also support limited diagenesis in these shells, since geochemical variations are strongly related to their restricted luminescence. Importantly, Fe/Ca, Mn/Ca and Mg/Ca mean values are usually higher in the luminescent zones, reflecting diagenetic enrichments during burial. It is not impossible, however, that diagenetic incorporation of Mg^{2+} into the shells, possibly derived from decomposition of volcaniclastic sediments to pore-fluids, could have been a secondary supplement to already originally high Mg^{2+} levels in the shells. In turn, Sr/Ca and Na/Ca ratios mainly present higher mean values in the less luminescent zones, which is suggestive of limited diagenetic modification. Therefore, part of the primary geochemical intra-shell variations in such zones may have been preserved. The unclear relationship of Ba/Ca ratios with the luminescence of the shells also implies partial retention of the original

https://doi.org/10.1017/S0954102006000411 Published online by Cambridge University Press

intra-shell variations.

Particularly indicative of weak diagenesis are the REE results provided, for the first time, from *A. rabotensis* whole-shells. These inoceramid REE contents are significantly lower than those from their host whole-rocks. In view of that, it is suggested that diagenesis affecting the whole-shell geochemistry (major, minor and trace elements) was principally influenced by the geochemical nature of the host rock, the latter modifying the availability of cations in pore-fluids through the diagenetic transformations of their main components.

As regards the inoceramid shell microstructure, only *A. rabotensis* has been shown to exhibit marked growth breaks. These breaks, interrupting the continuous and cyclic shell growth of still unknown periods in inoceramids, have been interpreted as reflecting conditions of strong palaeoenvironmental stress, which could have finally led to the early inoceramid disappearance in southern high latitudes (10 m.y. before the K/T boundary in Antarctica). As new evidence, we propose the possibility of the characteristic alternating aragonitic and calcitic thin sublayers, which form the inner aragonitic nacreous layer, as being a response of inoceramids to severe changes in palaeoenvironmental conditions. This is supported by the exclusive occurrence of the particular inner aragonitic nacreous layer in *A. rabotensis*. Finally, before analysing for isotopic palaeotemperatures, we first recommend accurately evaluating possible mineralogical variability within the inoceramid shells, particularly in the case of the inner aragonitic nacreous layer. This is especially important when new isotopic data are proffered for deciphering inoceramid extinction from a worldwide perspective.

Acknowledgements

The present study has been sponsored by Research Projects PIP 2756 (CONICET, Argentina) and PICT 8675 (ANPCyT, Argentina) and by 9/UPV130.310-14596/2002 (University of the Basque-Country, Spain). E.B. Olivero is most grateful to C.A. Rinaldi, S. Marenssi, and Instituto Antártico Argentino for continued scientific and logistic support over the years. D.R. Martinioni, F. Mussel and G. Robles are also acknowledged for their friendship and support during several seasons of field research in Antarctica. The manuscript benefited greatly from useful comments by J.A. Crame, D. Pirrie, J. McArthur and G. Price. We express our thanks to C. Laurin for linguistic assistance and A.P.M. Vaughan for editorial handling.

References

Al-Aasm, I.S. & Veizer, J. 1982. Chemical stabilization of low-Mg calcite: an example of brachiopods. *Journal of Sedimentary Petrology*, **52**, 1101–1109.

Banner, J.L., Hanson, G.N. & Meyers, W.J. 1988. Rare earth element and Nd isotopic variations in the regionally extensive dolomites from the Burlington–Keouk Formation (Mississippian): implications for REE mobility during carbonate diagenesis. *Journal of Sedimentary Petrology*, **58**, 415–432.

Barrera, E. & Savin, S.M. 1999. Evolution of late Campanian–Maastrichtian marine climates and oceans. *Geological Society of America Special Paper*, **332**, 245–282.

Barrera, E., Huber, B.T., Savin, S.M. & Webb, P.N. 1987. Antarctic marine temperatures: Late Campanian through Early Paleocene. *Paleoceanography*, **2**, 21–47.

Barrera, E. & Huber, B.T. 1990. Evolution of Antarctic bottom waters during the Maastrichtian: foraminifer oxygen and carbon isotope ratios, leg 113. *In* Baker, P.F., Kennet, J.P. & 25 Others, *eds. Proceedings of the Ocean Drilling Program, Scientific Results, Leg 113*. Washington, DC: US Government Printing Office, 813–827.

Brand, U. & Veizer, J. 1980. Chemical diagenesis of a multicomponent carbonate system. 1. Trace elements. *Journal of Sedimentary Petrology*, **50**, 1219–1236.

Brand, U. & Morrison, J.O. 1987. Biogeochemistry of fossil marine invertebrates. *Geoscience Canada*, **14**, 85–107.

Cande, S.C. & Kent, D.V. 1995. Revised calibration of the geomagnetic polarity timescale for the Late Cretaceous and Cenozoic. *Journal of Geophysical Research*, **100**, 6093–6095.

Chauris, H., LeRossuseau, J., Beaudoin, B., Propson, S. & Montarani, A. 1998. Inoceramid extinction in the Gubbio basin (northeastern Apennines of Italy) and relations with mid-Maastrichtian environmental changes. *Palaeogeography, Palaeoclimatology, Palaeoecology*, **139**, 177–193.

Clarke, A. 1990. Temperature and evolution: southern ocean cooling and the Antarctic marine fauna. *In* Kerry, K.R. & Hempel, G., *eds. Antarctic ecosystems: ecological change and conservation*. Berlin: Springer, 9–22.

Crame, J.A. 1983. Lower Cretaceous bivalve biostratigraphy of Antarctica. *Zitteliana*, **10**, 399–406.

Crame, J.A. & Luther, A. 1997. The last inoceramid bivalves in Antarctica. *Cretaceous Research*, **18**, 179–195.

Crame, J.A., Lomas, S.A., Pirrie, D. & Luther, A. 1996. Late Cretaceous extinction patterns in Antarctica. *Journal of the Geological Society, London*, **153**, 503–506.

Crame, J.A., Francis, J.E., Cantrill, D.J. & Pirrie, D. 2004. Maastrichtian stratigraphy of Antarctica. *Cretaceous Research*, **25**, 411–423.

Crame, J.A., Pirrie, D., Riding, J.B. & Thomson, M.R.A. 1991. Campanian–Maastrichtian (Cretaceous) stratigraphy of the James Ross Island area, Antarctica. *Journal of the Geological Society, London*, **148,** 1125–1140.

D'Hondt, S.A. & Lindinger, M. 1994. A stable isotopic record of the Maastrichtian ocean-climate system: South Atlantic DSDP site 528. *Palaeogeography, Palaeoclimatology, Palaeoecology*, **112**, 363–378.

Dingle, R.V. & Lavelle, M. 1998. Late Cretaceous–Cenozoic climatic variations of the northern Antarctic Peninsula: new geochemical evidence and review. *Palaeogeography, Palaeoclimatology, Palaeoecology*, **141**, 215–232.

Ditchfield, P.W., Marshall, J.D. & Pirrie, D. 1994. High latitude palaeo-temperature variation: new data from the Tithonian to Eocene of James Ross Island, Antarctica. *Palaeogeography, Palaeoclimatology, Palaeoecology*, **107**, 79–101.

Elorza, J. & García-Garmilla, F. 1996. Petrologic and geochemical evidence for diagenesis of inoceramid bivalve shells in the Plentzia Formation (Upper Cretaceous, Basque–Cantabrian Region, Northern Spain). *Cretaceous Research*, **17**, 479–503.

ELORZA, J. & GARCÍA-GARMILLA, F. 1998. Palaeoenvironmental implications and diagenesis of inoceramid shells (Bivalvia) in the mid-Maastrichtian beds of the Sopelana, Zumaya and Bidart sections (coast of the Bay of Biscay, Basque Country). *Palaeogeography, Palaeoclimatology, Palaeoecology*, **141,** 303–328.

ELORZA, J., GARCÍA-GARMILLA, F. & JAGT, J.W.M. 1997. Diagenesis-related differences and elemental composition of late Campanian and early Maastrichtian inoceramids and belemnites from NE Belgium: palaeoenvironmental implications. *Netherlands Journal of Geoscience/Geologie in Mijnbouw*, **75**, 349–360.

ELORZA, J., GÓMEZ-ALDAY, J.J. & OLIVERO, E.B. 2001. Environmental stress and diagenesis modifications in inoceramids and belemnites from the Upper Cretaceous James Ross Island, Antarctica. *Facies*, **44**, 227–242.

FISHER, C.G. & ARTHUR, M.A. 2002. Water mass characteristics in the Cenomanian US Western Interior seaway as indicated by stable isotopes of calcareous organisms. *Palaeogeography, Palaeoclimatology, Palaeoecology*. **188**, 189–213.

FRANCIS, J.E. 1986. Growth rings in Cretaceous and Tertiary wood from Antarctica and their palaeoclimatic implications. *Palaeontology*, **29**, 665–684.

FRANCIS, J.E. 1989. Palaeoclimatic significance of Cretaceous–early Tertiary fossil forests of the Antarctic Peninsula. *In* THOMSON, M.R.A., CRAME, J.A. & THOMSON, J.W., *eds. Geological evolution of Antarctica*. Cambridge: Cambridge University Press, 623–627.

FRANK, T.D. & ARTHUR, M.A. 1999. Tectonic forcings of Maastrichtian ocean-climate evolution. *Paleoceanography*, **14,** 103–117.

GÓMEZ-ALDAY, J.J. 2002. *Inocerámidos (Bivalvia): diagénesis e implicaciones paleoambientales. Maastrichtiense inferior*. PhD thesis, University of the Basque-Country, 232 pp. [Unpublished]

GÓMEZ-ALDAY, J.J. & ELORZA, J. 2003. Diagenesis, regular growth and records of seasonality in inoceramids bivalve shells from mid-Maastrichtian hemipelagic beds of the Bay of Biscay. *Netherlands Journal of Geoscience/Geologie in Mijnbouw*, **82**, 289–301.

GÓMEZ-ALDAY, J.J., LÓPEZ, G. & ELORZA, J. 2004. Evidence of climatic cooling at the Early/Late Maastrichtian boundary from inoceramid distribution and isotopes. Sopelana sections, Basque Country, Spain. *Cretaceous Research*, **25**, 649–668.

GONZÁLEZ-CASADO, J.M., JIMÉNEZ-BERROCOSO, A., GARCÍA-CUEVAS, C. & ELORZA, J. 2003. Strain determinations using inoceramid shells as strain markers: comparison of the calcite strain gauge technique and the Fry method. *Journal of Structural Geology*, **25**, 1773–1778.

GOVINDARAJU, K. & MEVELLE, G. 1987. Fully automated dissolution and separation methods for inductively coupled plasma atomic emission spectrometry rock analysis. Application to determination of rare earth elements. *Journal of Analytical Atomic Spectrometry*, **2**, 615–621.

GRANDJEAN, P. & ALBARÈDE, F. 1989. Rare earth elements in old biogenic apatite. *Geochimica et Cosmochimica Acta*, **57**, 2507–2514.

HAGGART, J.W. & BUSTIN, R.M. 1999. Selective replacement of mollusk shell by chlorite, Lower Cretaceous Longarm Formation, Queen Charlotte Island, British Columbia. *Canadian Journal of Earth Science*, **36**, 333–338.

HALEY, B.A., KLINKHAMMER, G.P. & MCMANUS, J. 2004. Rare earth elements in pore waters of marine sediments. *Geochimica et Cosmochimica Acta*, **68**, 1265–1279.

HARRINGTON, R.J. 1986. *Growth patterns within the genus Protohaca (Bivalvia: Veneridae) from the Gulf of Alaska to Panama: palaeotemperatures, palaeobiogeography and palaeolatitudes*. PhD thesis, University of California, 235 pp. [Unpublished.]

HILBRECHT, H., FIREG, C., TRÖGER, K.A., VOIGT, S. & VOIGT, T. 1996. Shallow water facies during the Cenomanian-Turonian anoxic events: bio-events, isotopes, and sea level in southern Germany. *Cretaceous Research*, **17**, 229–253.

HUBER, B.T. 1998. Tropical paradise at the Cretaceous poles? *Science*, **282**, 2199–2200.

HUBER, B.T. & WATKINS, D.K. 1992. Biogeography of Campanian–Maastrichtian calcareous plankton in the region of the Southern Ocean: paleogeographic and paleoclimatic implications. *Antarctic Research Series*, **56**, 31–60.

HUBER, B.T., HODELL, D.A. & HAMILTON, C.P. 1995. Middle–Late Cretaceous climate of the southern high latitudes: stable isotopic evidence for minimal equator-to-pole thermal gradients. *Geological Society of America Bulletin*, **107**, 1164–1191.

HUBER, B.T., NORRIS, R.D. & MACLEOD, K.G. 2002. Deep-sea paleotemperature record of extreme warmth during the Cretaceous. *Geology*, **30**, 123–126.

INESON, J.R. 1989. Coarse-grained submarine fan and slope apron deposits in a Cretaceous back-arc basin, Antarctica. *Sedimentology*, **36**, 793–819.

JIMÉNEZ-BERROCOSO, A. 2004. *Petrología y geoquímica de inocerámidos (Bivalvia) y roca encajante en facies de plataforma y cuenca profunda (Coniaciense final-Santoniense superior, Cuenca Vasco-Cantábrica): contrastes diagenéticos e implicaciones paleoambientales*. PhD thesis, Press Service, University of the Basque-Country, 459 pp.

JIMÉNEZ-BERROCOSO, A., ZULUAGA, M.C. & ELORZA, J. 2004. Minor- and trace-element intra-shell variations in Santonian inoceramids (Basque–Cantabrian Basin, northern Spain): diagenetic and primary causes. *Facies*, **50**, 35–60.

KENNISH, M.J. 1980. Shell microgrowth analysis. *Mercenaria mercenaria* as a type example for research in population dynamics. *In* LUTZ, R.A. & RHOADS, D.C., *eds. Skeletal growth of aquatic organisms*. New York: Plenums Press, 255–294.

LAWRENCE, J.R., DREVER, J.I., ANDERSON, T.F. & BRUECKNER, H.K. 1979. Importance of alteration of volcanic material in the sediments of Deep Sea Drilling Site 323: chemistry, $^{18}O/^{16}O$ and $^{87}Sr/^{86}Sr$. *Geochimica et Cosmochimica Acta*, **43**, 537–588.

LÉCUYER, C., BOGEY, C., GARCÍA, J.P., GRANDJEAN, P., BARRAT, J.A., FLOQUET, M., BARDET, N. & PEREDA-SUBERBIOLA, X. 2003. Stable isotope composition and rare earth element content of vertebrate remains form the Late Cretaceous of northern Spain (Laño): did the environmental record survive? *Palaeogeography, Palaeoclimatology, Palaeoecology*, **193**, 457–471.

LÉCUYER, C., REYNARD, B. & GRANDJEAN, P. 2004. Rare earth element evolution of Phanerozoic seawater recorded in biogenic apatites. *Chemical Geology*, **204**, 63–102.

LI, L. & KELLER, G. 1999. Variability in Late Cretaceous climate and deep waters: evidence from stable isotopes. *Marine Geology*, **161**, 171–190.

LIRIO, J.M., MARENSSI, S.A., MARSHALL, P.A., SANTILLANA, S.N. & RINALDI, C.A. 1989. Marambio Group at the southeastern part of James Ross Island, Antarctica. *Instituto Antártico Argentino Contribución*, **371**, 46 pp.

LUTZ, R.A. & RHOADS, D.C. 1977. Anaerobiosis and a theory of growth line formation. *Science*, **198**, 1222–1227.

MACELLARI, C.E. 1986. Late Campanian–Maastrichtian ammonite fauna from Seymour Island (Antarctic Peninsula). *The Paleontological Society Memoir*, **18**, 1–55.

MACELLARI, C.E. 1988. Stratigraphy, sedimentology and paleoecology of Upper Cretaceous/Paleocene shelf-deltaic sediments of Seymour Island (Antarctic Peninsula). *Geological Society of America, Memoir*, **169**, 25–53.

MACHEL, H.G. 1985. Cathodoluminescence in calcite and dolomite and its chemical interpretation. *Geoscience Canada*, **12**, 139–147.

MACHEL, H.G. 2000. Application of cathodoluminescence to carbonate diagenesis. *In* PAGEL, M.G., BARBIN, V., BLANC, P. & OHNENSTETTER, D., *eds*. *Cathodoluminescence in Geosciences*. Berlin: Springer, 271–301.

MACLEOD, K.G. 1994a. Bioturbation, inoceramid extinction, and mid-Maastrichtian ecological change. *Geology*, **22**, 139–142.

MacLeod, K.G. 1994b. Extinction of inoceramid bivalves in Maastrichtian strata of the Bay of Biscay Region of France and Spain. *Journal of Paleontology*, **68**, 1048–1066.

MacLeod, K.G. & Huber, B.T. 1996. Reorganization of deep ocean circulation accompanying a Late Cretaceous extinction event. *Nature*, **380**, 422–425.

MacLeod, K.G., Huber, B.T. & Le Ducharme, M. 2000. Paleontological and geochemical constraints on changes in the deep ocean during the Cretaceous greenhouse interval *In* Huber, B.T., MacLeod, K.G. & Wing, H., *eds*. *Warm climates in Earth history*. Cambridge: Cambridge University Press, 241–274.

MacLeod, K.G., Huber, B.T. & Ward, P.D. 1996. The biostratigraphy and paleobiogeography of Maastrichtian inoceramids. *Geological Society of America, Special Paper*, **307**, 361–373.

Marenssi, S.A., Lirio, J.M., Santillana, S.N., Martinioni, D.R. & Palamarczuk, S. 1992. The Upper Cretaceous of southeastern James Ross Island, Antarctica. Geología de la Isla James Ross. *In* Rinaldi, C.A., *ed. Geología de la Isla James Ross*. Buenos Aires: Instituto Antártico Argentino. Dirección Nacional del Antártico, 89–100.

Marshall, J.D., Ditchfield, P.W. & Pirrie, D. 1993. Stable isotope palaeo-temperatures and the evolution of high palaeolatitude climate in the Cretaceous. *In* Jones, P.D. & Wigley, T.M.L., *eds*. *Antarctic Special Topic*. Cambridge: British Antarctic Survey, 71–79.

McLennan, S.M. 1989. Rare earth elements in sedimentary rocks: influence of provenance and sedimentary processes. *Reviews in Mineralogy*, **21**, 169–200.

Medina, F. & Buatois, L. 1992. Bioestratigrafia del Aptiano–Campaniano (Cretácico superior) en la Isla James Ross. *In* Rinaldi, C.A., *ed. Geología de la Isla James Ross*. Buenos Aires: Instituto Antártico Argentino. Dirección Nacional del Antártico, 37–47.

Nockolds, S.R., Knox, R.W.O'B. & Chinner, G.A. 1979. *Petrology for students*. Cambridge: Cambridge University Press, 435 pp.

Olivero, E.B. 1992. Asociaciones de ammonites de la Formación Santa Marta (Cretácico tardío), Isla James Ross, Antártida. *In* Rinaldi, C.A., *ed. Geología de la Isla James Ross*. Buenos Aires: Instituto Antártico Argentino. Dirección Nacional del Antártico, 47–76.

Olivero, E.B. & Medina, F.A. 2000. Patterns of Late Cretaceous ammonite biogeography in southern high latitudes: the family Kossmaticeratidae in Antarctica. *Cretaceous Research*, **21**, 269–279.

Olivero, E.B. & Mussel, F.A. 1993. *Biofacies de "Inoceramus" (Bivalvia) en ambientes marinos proximales del Cretácico Superior de Antártida*. Segundas Jornadas de Comunicaciones sobre Investigaciones Antárticas, Instituto Antártico Argentino, Buenos Aires, 189–190.

Olivero, E.B., Martinioni, D.R. & Mussel, F.A. 1992. Upper Cretaceous sedimentology and biostratigraphy of western Cape Lamb (Vega Island, Antarctica). Implications on sedimentary cycles and evolution of the basin. *In* Rinaldi, C.A., *ed. Geología de la Isla James Ross*. Buenos Aires: Instituto Antártico Argentino. Dirección Nacional del Antártico, 147–164.

Olivero, E.B., Scasso, R.A. & Rinaldi, C.A. 1986. Revision of the Marambio Group, James Ross Island, Antarctica. *Contribuciones del Instituto Antártico Argentino*, **331**, 1–29.

Olivero, E.B., Malumián, N. & Palamarczuk, S. 2003. Estratigrafía del Cretácico Superior-Paleoceno del área de Bahía Thetis, Andes fueguinos, Argentina: acontecimientos tectónicos y paleobiológicos. *Revista Geológica de Chile*, **30**, 245–263.

Olivero, E.B., Malumián, N. & López C.M.I. 2004. Changes in bioturbation intensity near the inoceramid extinction horizon: new data from Antarctica and Tierra del Fuego. Ichnia 2004. *First International Congress on Ichnology*, Abstract Book, 63–64.

Olivero, E.B., Martinioni, D.R., Mussel, F.A. & Robles, G.M. 1999. *Estratigrafía del Santoniano-Maastrichtiano, Grupo Marambio, Cuenca James Ross, Antártida*. Cuartas Jornadas de Comunicaciones sobre Investigaciones Antárticas, Instituto Antártico Argentino, Buenos Aires, 257–261.

Palmer, M.R. 1985. Rare earth elements in foraminifera tests. *Earth and Planetary Science Letters*, **73**, 285–298.

Pirrie, D. 1991. Controls on the petrographic evolution of an active margin sedimentary sequence: the Larsen Basin, Antarctica. *Geological Society, London, Special Publication*, **57**, 231–249.

Pirrie, D. & Marshall, J.D. 1990a. Diagenesis of Inoceramus and Late Cretaceous paleoenvironmental geochemistry: a case study from James Ross Island, Antarctica. *Palaios*, **5**, 336–345.

Pirrie, D. & Marshall, J.D. 1990b. High-paleolatitude Late Cretaceous paleotemperatures: new data from James Ross Island, Antarctica. *Geology*, **18**, 31–34.

Pirrie, D., Crame, J.A., Lomas, S.A. & Riding, J.B. 1997. Late Cretaceous stratigraphy of the Admiralty Sound region, James Ross Basin, Antarctica. *Cretaceous Research*, **18**, 109–137.

Price, G.D. & Sellwood, B.W. 1997. "Warm" palaeotemperatures from high Late Jurassic palaeolatitudes (Falkland Plateau): Ecological, environmental or diagenetic controls? *Palaeogeography, Palaeoclimatology, Palaeoecology*, **129**, 315–327.

Qing, H. & Mountjoy, E.W. 1994. Rare earth element geochemistry of dolomites in the Middle Devonian Presqu'ile barrier, Western Canada Sedimentary Basin: implications for fluid-rock ratios during dolomitization. *Sedimentology*, **41**, 787–804.

Reynard, B., Lécuyer, C. & Grandjean, P. 1999. Crystal-chemical controls on rare-earth element concentrations in fossil biogenic apatites and implications for paleoenvironmental reconstructions. *Chemical Geology*, **155**, 233–241.

Saw, H.F. & Wasserburg, G.J. 1985. Sm–Nd in marine carbonates and phosphates: implications for Nd isotopes in seawater and crustal ages. *Geochimica et Cosmochimica Acta*, **49**, 503–518.

Scasso, R.A., Olivero, E.B. & Buatois, L. 1991. Lithofacies, biofacies, and ichnoassemblages evolution of a shallow submarine volcanoclastic fan-shelf depositional system. Upper Cretaceous, James Ross Island, Antarctica. *Journal of South American Earth Sciences*, **4**, 239–260.

Schönfeld, J., Siroko, F. & Jorgensen, N.O. 1991. Oxygen isotope composition of Upper Cretaceous chalk at Lägerdorf (NW Germany): its original environmental signal and palaeotemperature interpretation. *Cretaceous Research*, **12**, 27–46.

Spicer, R.A. & Corfield, R.M. 1992. A review of terrestrial and marine climates in the Cretaceous with implications for modelling the 'Greenhouse Earth'. *Geological Magazine*, **129**, 169–180.

Wang, Y.L., Liu, Y.G. & Schmitt, R.A. 1986. Rare earth element geochemistry of South Atlantic deep sea sediments: Ce anomaly change at 54 My. *Geochimica et Cosmochimica Acta*, **50**, 1337–1355.

Whittaker, S.G., Kyser, T.K. & Caldwell, W.G.E. 1987. Palaeoenvironmental geochemistry of the Claggett marine cyclotherm in south-central Saaskatchewan. *Canadian Journal of Earth Sciences*, **24**, 967–984.

Wright, E.K. 1987. Stratification and paleocirculation of the Late Cretaceous Western Interior Seaway of North America. *Geological Society of America Bulletin*, **99**, 480–490.

Zakharov, Y.D., Boriskina, N.G., Ignatyev, A.V., Tanabe, K., Shigeta, Y., Popov, A.M., Afanasyeva, T.B. & Maeda, H. 1999. Palaeotemperature curve for the Late Cretaceous of the northwestern circum-Pacific. *Cretaceous Research*, **20**, 685–697.

Zakharov, Y.D., Smyshlyaev, O.P., Tanabe, K., Shigeta, Y., Maeda, H., Ignatiev, A.V., Velivetskaya, T.A., Afanasyeva, T.B., Popov, A.M., Golozubov, V.V., Kolyada, A.A., Cherbadzhi, A.K. & Moriya, K. 2005. Seasonal temperature fluctuations in the high northern latitudes during the Cretaceous Period: isotopic evidence from Albian and Coniacian shallow-water invertebrates of the Talovka River Basin, Koryak Upland, Russian Far East. *Cretaceous Research*, **26**, 113–132.

Zinsmeister, W.J. & Feldmann, R.M. 1996. Late Cretaceous faunal changes in the high southern latitudes: a harbinger of global biotic catastrophe? *In* MacLeod, K.G. & Keller, G., *eds*. *Cretaceous–Tertiary mass extinctions: biotic and environmental changes*. New York: Norton, 303–325.